Environmental Science & Technology

pubs.acs.org/est

Article

Photochemical Production of Singlet Oxygen in Adirondack Long-Term Monitoring Lakes of Varying Browning Status

Birdem Öz, Philip K. Snyder, Xiaoyu Jiao, Charles T. Driscoll, and Teng Zeng*

Cite This: https://doi.org/10.1021/acs.est.5c04001

Read Online

ACCESS | Metrics & More | Article Recommendations | Supporting Information

ABSTRACT: Widespread browning of surface waters in boreal and temperate regions of the Northern Hemisphere has been documented through long-term monitoring of color or dissolved organic matter (DOM) over recent decades. While the ecological implications of browning have received considerable attention, its impacts on the photochemical production of reactive intermediates from DOM remain understudied despite their importance for biogeochemical processes and contaminant fate in sunlit surface waters. To address this gap, we investigated singlet oxygen ($^1O_2$) production in 37 lakes within the Adirondack Long-Term Monitoring (ALTM) program. Wavelet coherence tests confirmed the synchrony between dissolved organic carbon (DOC) and color as well as the time-scale-dependent influence of regional atmospheric and hydroclimatic factors on DOC dynamics in these lakes. Hydrogeological conditions of lake watersheds (e.g., hydrologic connectivity and surficial geology) and seasonal variations in DOM quality jointly shaped the spatiotemporal patterns of the apparent quantum yields of $^1O_2$. Within the euphotic zone, depth-averaged steady-state concentrations of $^1O_2$ were higher in lakes experiencing more intense browning, as operationally defined through trend analyses of long-term water chemistry data; however, the relevance of $^1O_2$-mediated reactions depends on the time scales of photochemical transformation relative to lake flushing. Overall, our study provides an initial assessment of $^1O_2$ production in relation to lake browning and highlights the need for long-term photochemical measurements for an improved assessment.

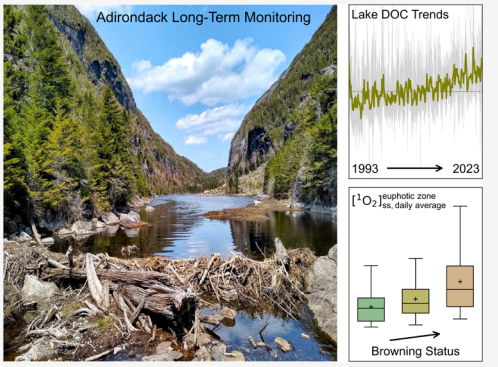

KEYWORDS: *browning, DOM, photochemistry, singlet oxygen, temperate lakes*

INTRODUCTION

Many surface water systems in the temperate and boreal regions of North America and Europe have experienced varying degrees of browning in recent decades—a shift in optical properties that gives the water a brownish hue and is often attributed to increasing concentrations of dissolved organic matter (DOM), as indicated by long-term records of color or dissolved organic carbon (DOC).[1−3] Multiple anthropogenic and hydroclimatic factors, including reduced atmospheric acid deposition,[4−6] changing precipitation regimes,[7,8] rising atmospheric temperatures and CO_2,[9,10] and evolving land use patterns (e.g., afforestation[11] and ditching[12]), have been put forward as potential drivers of browning, though their relative importance and interactions remain difficult to disentangle and may be further complicated by landscape heterogeneity.[13] Collectively, previous studies have established that browning has profound impacts on lake ecosystem functioning (e.g., carbon budgets,[14] primary productivity,[15] oxythermal habitat conditions[16])[17,18] while also posing operational challenges for water treatment by increasing coagulant demand, energy consumption, and byproduct formation.[19−23]

Considering the effects of browning on light attenuation and thermal stratification, prior research has explored its implications for the photochemical production of reactive intermediates from DOM in sunlit lakes.[24] For example, modeling of boreal lakes in Sweden projected that browning would lead to increases in steady-state concentrations of excited triplet states of DOM (^{3}DOM*) and singlet oxygen ($^1O_2$) down to 5 cm and the mean depth of each lake, thereby accelerating the indirect photodegradation of compounds that primarily react with these reactive intermediates.[25] Modeling of a smaller set of Nordic lakes also predicted that browning would enhance the formation of reactive oxygen species in the upper centimeters of the water column while inhibiting their production in deeper layers.[26] Together, these and related efforts[27,28] provided a theoretical assessment of reactive intermediate formation in the context of lake browning. Nonetheless, their modeling framework did not incorporate long-term monitoring records to define the extent of browning and relied on literature data or reference materials to

Received: March 26, 2025
Revised: June 23, 2025
Accepted: June 25, 2025

approximate the apparent quantum yields of reactive intermediates instead of lake-specific measurements.

To address this gap, we investigated the production of $^1O_2$ in the Adirondack Long-Term Monitoring (ALTM) lakes by integrating time series and trend analyses of long-term data sets with photochemical characterization of field-collected samples. Historically, the Adirondack region of New York was a hotspot for atmospheric acid deposition from industrial emissions.[5] To assess the recovery of Adirondack lakes from acidification, the ALTM program was launched in 1992 to monitor surface water chemistry in 52 lakes selected from a large-scale survey of 1469 lakes conducted between 1984 and 1987.[29,30] Lakes within the ALTM program thus represent an ideal set of acid-impacted systems draining remote forested watersheds for studying photochemistry in relation to browning. Leveraging long-term data sets, we applied wavelet coherence tests to examine synchronous dynamics between the time series of DOC and regional drivers previously hypothesized to influence browning across 37 ALTM lakes at different time scales, followed by seasonal Mann−Kendall trend analyses of DOC, color, and specific UV absorbance at 254 nm ($SUVA_{254}$)[31] to classify the browning status of these lakes. Concurrently, we analyzed the spatiotemporal patterns of apparent quantum yields of singlet oxygen ($\Phi_{app,^1O_2}$) for whole water samples collected from these lakes with respect to watershed hydrologic connectivity, surficial geology, and season. $^1O_2$ was selected as the focus of our work for its critical role in biogeochemical cycling,[32−36] transformations of organic micropollutants and bioactive secondary metabolites,[37−44] and pathogen inactivation,[45−47] among other processes, as well as its better-understood formation and deactivation mechanisms that facilitate the estimation of environmentally relevant concentrations for fate modeling.[48,49] To this end, we compared depth-averaged steady-state concentrations of $^1O_2$ in the euphotic zone of ALTM lakes based on their browning status and evaluated the half-lives of $^1O_2$-mediated reactions for selected contaminants relative to lake hydraulic residence times.

MATERIALS AND METHODS

Chemical sources and reagent preparation are described in the Supporting Information.

Field Sampling. Whole water samples were collected from 37 lakes (Figure S1) monitored through the ALTM program for water chemistry parameters (e.g., pH, DOC, dissolved inorganic carbon, specific conductance, acid neutralizing capacity, acid anions, base cations, and speciated aluminum).[29] $SUVA_{254}$ has also been monitored in these lakes since 2013.[50] Of the lakes sampled, 35 are headwater or chain drainage lakes situated in watersheds with predominantly thin, medium, or thick deposits of glacial till, while the remaining two are mounded seepage lakes.[51] Most lakes are surrounded by a mix of deciduous forest, coniferous forest, and deciduous-coniferous forest, with some also bordered by shrub-sapling habitats and wetlands, whereas open grasslands, agricultural fields, and developed areas are minimal.[29] Overall, these lakes exhibit a range of morphometric characteristics and watershed attributes (Table S1). Whole water samples (n = 129) were collected over three seasons (Table S2): fall−winter (October−November 2022), spring−summer (May−June 2023), and summer−fall (September 2023) under dry weather conditions. Samples were taken (e.g., using a Kemmerer sampler) at a depth of 0.5 m from the deepest part of each lake (37 samples per season), and in six cases, paired samples were also grabbed from outlet streams of a subset of drainage lakes (6 samples per season) for comparison. Samples were shipped in coolers to Syracuse University as soon as practically possible, filtered through 0.2-μm poly(ether sulfone) membranes, and stored under 4 °C until analysis. Field blanks (n = 9) were collected and processed with each batch of samples.

Sample Analysis. Water chemistry parameters were analyzed by the U.S. Geological Survey Soil and Low-Ionic-Strength Water Quality Laboratory (Troy, NY). Optical properties, such as Napierian absorption coefficient at 440 nm (a_{440}),[52] $SUVA_{254}$,[31] *E2:E3* (the ratio of Napierian absorption coefficients at 250 and 365 nm),[53] spectral slope coefficients (e.g., $S_{290-400}$ and $S_{300-600}$),[54,55] fluorescence index (FI),[56] humification index (HIX),[57] freshness index (β:α),[58] as well as total dissolved iron ([Fe]), were measured at Syracuse University. Water chemistry and optical data are summarized in Tables S3 and S4.

Photochemistry Experiments. Photolysis experiments were performed at least in duplicate using an Atlas Suntest XLS +(II) solar simulator equipped with a 1700 W xenon arc lamp and a daylight glass 300 nm UV filter. The lamp irradiance was controlled at 320 W/m^2 between 300 and 800 nm, and the solar simulator chamber temperature was maintained at 25 ± 1 °C with an Atlas SunCool chiller. Prior to irradiation, filtered samples were standardized to a DOC of 4.0 mg C/L when applicable (samples with DOC below this threshold were analyzed at their ambient DOC)[59] and spiked with furfuryl alcohol (FFA) as a probe to measure $^1O_2$ production,[60,61] along with 0.1 mM of methanol to quench hydroxyl radicals ($^•$OH).[62] Samples were then transferred to quartz test tubes (100 mm × 11 mm i.d.; held at ∼30° from the horizontal) and irradiated inside the solar simulator with bimolecular *p*-nitroanisole/pyridine actinometer solutions (to monitor the incident light intensity[63,64]). Solutions of Suwannee River natural organic matter (SRNOM; 2R101N), Suwannee River fulvic acid (SRFA; 3S101F), and Suwannee River humic acid (SRHA; 3S101H) were also irradiated as reference samples.

$\Phi_{app,^1O_2}$ were calculated over the wavelength range of 290−550 nm and combined with daily average solar irradiance to estimate the depth-averaged steady-state concentrations of $^1O_2$ in the euphotic zone ($[^1O_2]^{euphotic\ zone}_{ss,daily\ average}$) for each lake on the corresponding sampling dates using eq 1:[48,65,66]

$$[^1O_2]^{euphotic\ zone}_{ss,daily\ average} = \frac{\Phi_{app,^1O_2}}{k_d^{\Delta}} \times CF \times \sum_{\lambda=290nm}^{550nm} \frac{Z_{\lambda,daily\ average}}{z_{euphotic\ zone}} \times (1 - e^{-K_{d,\lambda} z_{euphotic\ zone}}) \times (1 - f_{backscatter}) \times f_{abs,CDOM} \quad (1)$$

where $\Phi_{app,^1O_2}$ (mol mol-photons^{-1}) is the apparent quantum yield of $^1O_2$, k_d^{Δ} (s^{-1}) is the pseudo-first-order deactivation rate constant of $^1O_2$ by water,[61] CF is the nonclear-sky correction factor for solar irradiance in the Adirondack region (i.e., 0.60 ± 0.06),[66] $Z_{\lambda,daily\ average}$ (10^{-3} mol-photons cm^{-2} s^{-1} nm^{-1}) is the site-specific daily average solar irradiance at a given wavelength λ modeled using the *Simple Model of the Atmospheric Radiative Transfer of Sunshine (SMARTS) v2.9.9* (Table S5)[67−69] with adjustments made for reflection off the water surface and increased path length within the water column,[63,65,70] $z_{euphotic\ zone}$ (cm) is the euphotic zone depth estimated using

https://doi.org/10.1021/acs.est.5c04001
Environ. Sci. Technol. XXXX, XXX, XXX−XXX

an empirical relationship established for Adirondack lakes (i.e., $z_{\text{euphotic zone}} = 4.6/[0.15[\text{DOC}]^{1.08}] \times 100$),[71] $K_{d,\lambda}$ (cm^{-1}) is the diffuse attenuation coefficient modeled following the relationship developed using UV wavelengths (i.e., $K_{d,\lambda} = \exp(-0.01347\lambda + 5.36[\text{DOC}]^{0.157})$),[72] $f_{\text{backscatter}}$ is the fraction of sunlight backscattered out of the water column,[48] and $f_{\text{abs,CDOM}}$ is the fraction of lake water absorbance attributable to colored DOM (CDOM).[48] Complete details of the photochemistry experiments and related calculations are provided in Sections S6−S8.

Data Analysis. Long-term water chemistry data (June 1992 to September 2023) for the 37 ALTM lakes were retrieved from the U.S. Geological Survey (USGS) National Water Information System[50] and imported into *Colab Pro* (Google) for analysis using *Python* or *R*. To investigate synchrony between the time series of DOC and four external drivers (preselected from a larger set of variables based on a variance inflation factor threshold of 2.0 to minimize collinearity[73]), including summed wet deposition of sulfate and nitrate, precipitation, soil wetness, and solar irradiance, across all lakes, wavelet coherence tests were performed using the *wsyn* package[74] over short (3−6 months), intermediate (12−24 months), and long (36−72 months) time scale bands (Table S6). Monthly wet deposition data for sulfate and nitrate were averaged from four Adirondack monitoring sites within the National Atmospheric Deposition Program's National Trends Network.[75] Monthly total precipitation data were retrieved from the Parameter-elevation Regressions on Independent Slopes Model (PRISM) Climate Group[76] using the *prism* package.[77] Monthly all-sky surface shortwave downward irradiance and root zone soil wetness data were retrieved from the National Aeronautics and Space Administration's Langley Research Center Prediction of Worldwide Energy Resource (POWER) Project[78] using the *nasapower* package.[79,80] Each time series was detrended, Box-Cox transformed, and standardized before analysis.[81] For every time scale band, the strength of association between two time series was quantified using a magnitude metric (ranging from 0 to 1), with a phase metric (ranging from $-\pi$ to π) further derived to characterize the relationship as positive in-phase ($-\pi/4$ to $\pi/4$), lagged positive ($-3\pi/4$ to $-\pi/4$), lagged negative ($\pi/4$ to $3\pi/4$), or negative antiphase ($3\pi/4$ to π or $-\pi$ to $-3\pi/4$).[81−83] Wavelet linear modeling was then applied to quantify the proportion of synchrony explained by time scale-specific relationships between DOC and statistically significant drivers and to assess their independent contributions and potential interactions (Table S7).[81]

To evaluate directional trends and rates of change in DOC and other water chemistry parameters (e.g., color and SUVA_{254}), the nonparametric seasonal Mann−Kendall test[84] was performed using the *pyMannKendall* package[85] to calculate Sen's slopes for the time series of each lake (based on the full extent of data available).[86] Sen's slopes with $p < 0.05$ were interpreted as statistically significant indicators of either increasing or decreasing trends, whereas those with $p \geq 0.05$ were considered insignificant and replaced with zeros (Table S8).[87] Sen's slopes were further standardized for k-means clustering to classify the browning status of ALTM lakes.

Statistical analyses (e.g., the Kruskal−Wallis test, Mann−Whitney *U* test, Spearman's correlation analysis, and generalized additive modeling) were performed using the *stats*[88] and *mgcv*[89] packages.

RESULTS AND DISCUSSION

Mechanisms Regulating DOC Dynamics. To test the hypothesis that browning in ALTM lakes responds to temporal changes in DOM, wavelet coherence tests were first performed to evaluate the synchrony between the time series of color and DOC as a function of time scale. Coherences between color and DOC were significant (band-aggregated $p < 0.0001$−0.006) and positive in-phase (mean phase 0.013−0.160) with comparable magnitudes (0.56 ± 0.02−0.64 ± 0.07) across three time scale bands (Figure 1a), confirming the temporally persistent nature of their synchrony. On average, a 0.095 ± 0.038 mg C/L change in DOC corresponded to a one-unit shift in color on the platinum−cobalt scale for ALTM lakes, which compared well with the value of 0.098 ± 0.043 mg C/L per platinum−cobalt unit derived from a large-scale survey of Adirondack lakes that preceded the ALTM program.[30]

To probe mechanisms influencing DOC trends, wavelet coherence tests were further performed to characterize time scale-specific synchrony between DOC and four external drivers representing regional atmospheric and hydroclimatic conditions, including acid deposition (i.e., the summed wet deposition of sulfate and nitrate), precipitation, soil wetness, and solar irradiance (Figure 1b−e). Wavelet linear modeling was then applied with DOC as the response variable to quantify the proportion of synchrony attributable to its relationships with these drivers (Figure 1f).[81] Over short time scales, all four drivers were statistically significant contributors, but only precipitation accounted for >10% of synchrony. Consistent with earlier findings,[81,90] precipitation showed a lagged negative relationship with DOC (mean phase 1.91), likely reflecting the joint influence of dilution (e.g., event-driven inputs of low-DOM upland runoff that bypass organic-rich soil horizons) and flushing (e.g., reduced hydraulic residence times that limit the retention and accumulation of DOM) within lakes.[91−93] Over intermediate time scales, the four drivers collectively explained 81% of synchrony, with solar irradiance contributing the largest fraction (39%), followed by soil wetness (30%), precipitation (18%), and acid deposition (17%). Solar irradiance exhibited a negative antiphase relationship with DOC (mean phase 3.06), underscoring the importance of in-lake photodegradation as a sink for DOM (e.g., through mineralization to carbon dioxide).[94,95] Meanwhile, soil wetness showed a lagged positive relationship with DOC (mean phase −1.31), as expected for increased DOM production and leaching driven by microbial activity under redox oscillations associated with drying−rewetting cycles.[96] Precipitation and acid deposition both exhibited a lagged negative relationship with DOC (mean phase 1.35), supporting the notion that declines in atmospheric acid deposition alter the acidity of soils and/or the ionic strength of soil solutions,[1] thereby enhancing DOM solubility and mobility. For instance, deprotonation of more acidic functional groups increases the net negative surface charge of DOM as soils become less acidic, while lower ionic strength concurrently reduces cation bridging and aggregation of DOM.[97,98] Over long time scales, precipitation and acid deposition were the only statistically significant drivers that explained 60% of synchrony. Contrary to the phase relationships observed at shorter time scales, precipitation showed a lagged positive relationship with DOC (mean phase −0.87) as previously noted,[6,81] suggesting that under extended precipitation regimes, enhanced hydrologic connectivity across the

https://doi.org/10.1021/acs.est.5c04001
Environ. Sci. Technol. XXXX, XXX, XXX−XXX

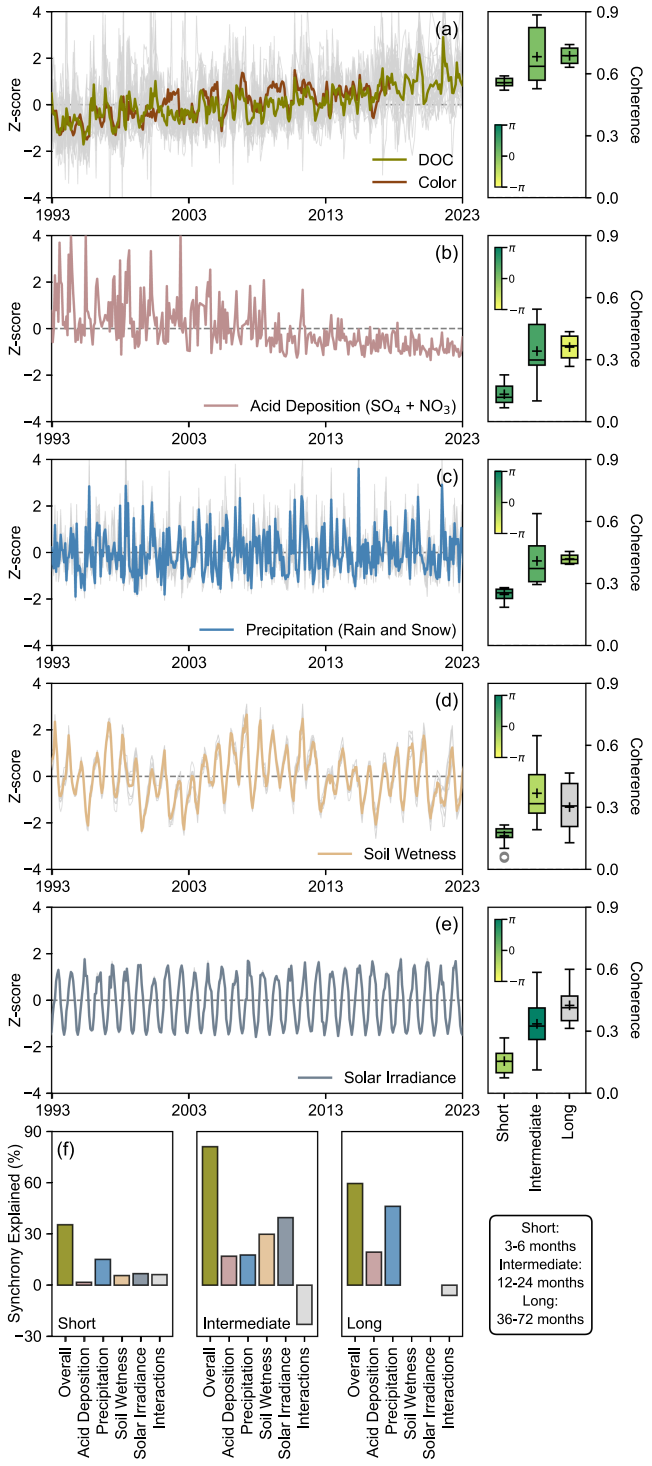

Figure 1. Wavelet coherences between the time series of DOC and regional drivers across 37 ALTM lakes over short (3−6 months), intermediate (12−24 months), and long (36−72 months) time scale bands: (a) Z-score-standardized time series of DOC and color for ALTM lakes along with coherence magnitudes and phase relationships for three time scales (Figure S5). Note that color data collection discontinued after 2017. (b) Z-score-standardized time series of the summed sulfate (SO_4) and nitrate (NO_3) wet deposition for ALTM lakes along with coherence magnitudes and phase relationships for three time scales (Figure S6). (c) Z-score-standardized time series of precipitation for ALTM lakes along with coherence magnitudes and phase relationships for three time scales (Figure S7). (d) Z-score-standardized time series of root zone soil wetness for ALTM lakes along with coherence magnitudes and phase relationships for three time scales (Figure S8). (e) Z-score-standardized time series of solar irradiance for ALTM lakes along with coherence magnitudes and phase relationships for three time scales (Figure S9). On panels (a)−(e), the solid line represents the site-average Z-score time series, while gray lines represent site-specific time series when available. Coherence magnitudes are normalized between 0 and 1, and phase relationships are classified as follows: positive in-phase ($-\pi/4$ to $\pi/4$), lagged positive ($-3\pi/4$ to $-\pi/4$), lagged negative ($\pi/4$ to $3\pi/4$), and negative antiphase ($3\pi/4$ to π or $-\pi$ to $-3\pi/4$).[83] On panels (d) and (e), the gray box in the boxplot indicates statistically insignificant coherence. (f) Synchrony explained by statistically significant drivers across the three time scales based on wavelet linear modeling (Table S7). Gray bars represent interacting effects among drivers.

terrestrial−aquatic interface may promote DOM export to lakes by activating subsurface flow paths (e.g., those intersecting organic-rich soil horizons[99]) and expanding source areas (e.g., those otherwise hydrologically disconnected during prolonged dry periods[100]).[101] Together, these results provide insights into the time-scale-specific and time-lagged processes driving DOC dynamics in ALTM lakes that cannot be readily resolved by standard correlation metrics.

Classification of Lake Browning Status. To classify the browning status of ALTM lakes, Sen's slopes for the time series of DOC, color, and $SUVA_{254}$ were calculated to determine the direction and magnitude of temporal changes. Most lakes (i.e., 33 out of 37) showed statistically significant positive slopes for DOC (0.005−0.105 mg C/L-year; $p < 0.0001$−0.0042; Figure S11), with a median value of 0.057 mg C/L-year similar to those recorded for lakes in eastern Canada (e.g., 0.05 mg C/L-year)[14,102] and over 400 headwater lakes and streams in Europe and North America (e.g., 0.04 mg C/L-year).[2] Sen's slopes for DOC were positively correlated with those for pH (Spearman's $\rho = 0.481$; $p < 0.0001$) but negatively correlated with those for the summed sulfate and nitrate concentrations ($\rho = -0.607$; $p < 0.0001$), reinforcing the link between recovery from acidification in ALTM lakes and their long-term DOC trends. Color also increased in 90% of the lakes with a median slope of 0.027 m^{-1}/year (converted to Napierian absorption coefficient at 440 nm[52]), which was equivalent to a 2.2% annual increase that exceeded rates (e.g., 1.1−1.6%/year) estimated for browning lakes in southern Sweden[11] and eastern Canada.[14] Cross-regional comparisons were intended to contextualize the rates of temporal change in DOC and color for ALTM lakes within the broader spectrum of values reported in the literature rather than to infer shared underlying mechanisms given the environmental heterogeneity among systems. Somewhat contrary to the trends of DOC and color, $SUVA_{254}$ either declined or remained mostly stable over the past decade. Multiple studies, such as those on acid-impacted streams in upland catchments in Scotland,[103] temperate lakes at the North Temperate Lakes Long-Term Ecological Research site in northern Wisconsin,[104] and boreal lakes on the Boreal Plains of western Canada,[105] have also observed divergent trends between DOC and $SUVA_{254}$, which may stem from their differential responses to shifting source contributions (e.g., disproportionate mobilization of low-aromatic DOM from mineral soil horizons[106,107]) and/or changing processing mechanisms (e.g., preferential loss of aromatic DOM moieties via in-lake decomposition and flocculation[108]). Varying degrees of temporal (de)coupling among Sen's slopes for DOC, color, and $SUVA_{254}$ suggest that, while biogeochemically

https://doi.org/10.1021/acs.est.5c04001
Environ. Sci. Technol. XXXX, XXX, XXX−XXX

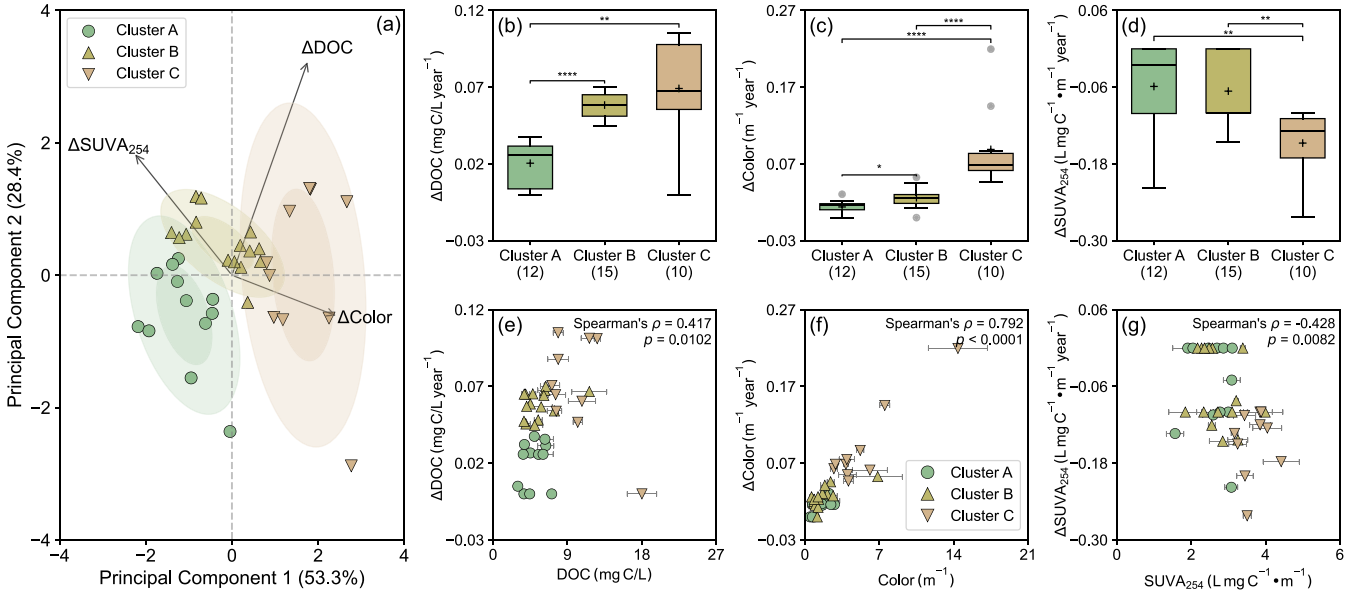

Figure 2. Classification of ALTM lakes by Sen's slopes of the time series of DOC, color, and $SUVA_{254}$ for multiple comparisons and Spearman's correlation analysis: (a) K-means clustering of lakes based on their Sen's slopes for DOC, color, and $SUVA_{254}$ (Table S8). Ellipses represent bivariate confidence intervals derived from the covariance structure of the data. The inner ellipse corresponds to the 68% confidence interval (one standard deviation), while the outer ellipse represents the 95% confidence interval (two standard deviations). (b) Multiple comparisons of Sen's slopes for DOC (data available from 1992 to 2023) across lake clusters. (c) Multiple comparisons of Sen's slopes for color (data available through 2017) across lake clusters. (d) Multiple comparisons of Sen's slopes for $SUVA_{254}$ (data available from 2013 onward) across lake clusters. (e) Spearman's correlation between Sen's slopes for DOC and DOC measured for ALTM samples. (f) Spearman's correlation between Sen's slopes for color and color (based on a_{440}) measured for ALTM samples. (g) Spearman's correlation between Sen's slopes for $SUVA_{254}$ and $SUVA_{254}$ measured for ALTM samples. On panels (b)−(d), each box spans the 25th to 75th percentiles, with whiskers extending to 1.5 times the interquartile range below the 25th and above the 75th percentiles. The centerline and "+" sign mark the median and mean, respectively. Gray circles represent outliers. Numbers in parentheses represent the number of lakes in each cluster. For multiple comparisons, a Kruskal−Wallis test was first performed to determine whether statistically significant differences existed among groups. If significant, pairwise Mann−Whitney *U* tests were performed, with significant differences marked by asterisks as "*" ($p < 0.05$), "**" ($p < 0.01$), "***" ($p < 0.001$), or "****" ($p < 0.0001$). On panels (e)−(g), error bars represent the standard deviations of measurements for samples from three sampling seasons; where absent, bars fall within symbols.

linked, these metrics do not necessarily serve as proxies for one another.

To provide a framework for interpreting $^1O_2$ formation in the context of browning, k-means clustering of Sen's slopes was performed to classify ALTM lakes into three clusters (Figure 2a). Overall, the slopes for DOC and color were more positive in clusters B and C than in cluster A lakes, whereas the slopes for $SUVA_{254}$ were less negative in clusters A and B than in cluster C lakes (Figure 2b−d). Color for ALTM samples analyzed in this work showed a stronger positive correlation with its Sen's slopes than DOC did with its corresponding slopes, whereas $SUVA_{254}$ was negatively correlated with its slopes (Figure 2e−g). Since lakes with faster increases in color and DOC but slower declines in $SUVA_{254}$ were more likely to feature darker water color, higher DOC, and more aromatic DOM, lakes in clusters A, B, and C were operationally designated as experiencing mild, moderate, and intense browning, respectively.

Spatiotemporal Patterns of $\Phi_{app,^1O_2}$. $\Phi_{app,^1O_2}$ for ALTM samples (n = 129) ranged from 0.6 to 3.7 × 10^{-2} mol mol-photons^{-1} (median 2.2 × 10^{-2}; Table S9) and fell within the range (0.5−10.9 × 10^{-2})[55,59,109−112] reported for whole water samples from temperate lacustrine systems in North America (Figure S12). To better contextualize the photoreactivity of ALTM lake waters, $\Phi_{app,^1O_2}$ were normalized against $\Phi^{SRNOM}_{app,^1O_2}$ measured in parallel as recommended by Ossola et al.[49] and aggregated for comparison with literature data on native or treated water samples across the freshwater-marine continuum, as well as DOM isolates, extracts, or fractions from diverse aquatic and terrestrial sources, compiled from 99 references (Table S18). Thirty-one of these references comeasured polychromatic and/or wavelength-specific $\Phi^{SRNOM}_{app,^1O_2}$ to allow for the harmonization of variations in $\Phi_{app,^1O_2}$. SRNOM was selected for normalization because it is more commonly analyzed than other reference materials in aquatic photochemistry studies despite differences in composition and photoreactivity relative to DOM in ALTM lakes. Overall, $\Phi_{app,^1O_2}/\Phi^{SRNOM}_{app,^1O_2}$ derived from the literature spanned over two orders of magnitude (0.06−33; median 1.05; n = 1068) due to heterogeneity in DOM origins, variability in sample treatment conditions, and uncertainties in the wavelength dependence of $\Phi_{app,^1O_2}$.[49] $\Phi_{app,^1O_2}/\Phi^{SRNOM}_{app,^1O_2}$ for ALTM samples ranged from 0.29 to 1.82 (median 1.12; Figure S13), which were not significantly different from ratios for whole water samples from other lacustrine environments (0.33−3.10; median 1.12; e.g., reservoirs in Japan[113]) and Nordic Reservoir NOM (0.47−1.93; median 1.12) but were lower than those for Pony Lake Fulvic Acid (0.22−5.51; median 1.57) and several other lacustrine DOM isolates or fractions from diverse geographic areas (0.13−3.74; median 1.55; e.g., U.S.,[114,115] Europe,[116] and polar regions[114,115]). Compared to other aquatic matrices, $\Phi_{app,^1O_2}/\Phi^{SRNOM}_{app,^1O_2}$ for ALTM samples were in the same range as ratios observed for riverine samples (0.06−3.96; median 1.13) but were lower than those for estuarine (0.89−3.92; median 2.10; e.g., the Florida Everglades[115,117]) and marine samples

https://doi.org/10.1021/acs.est.5c04001
Environ. Sci. Technol. XXXX, XXX, XXX−XXX

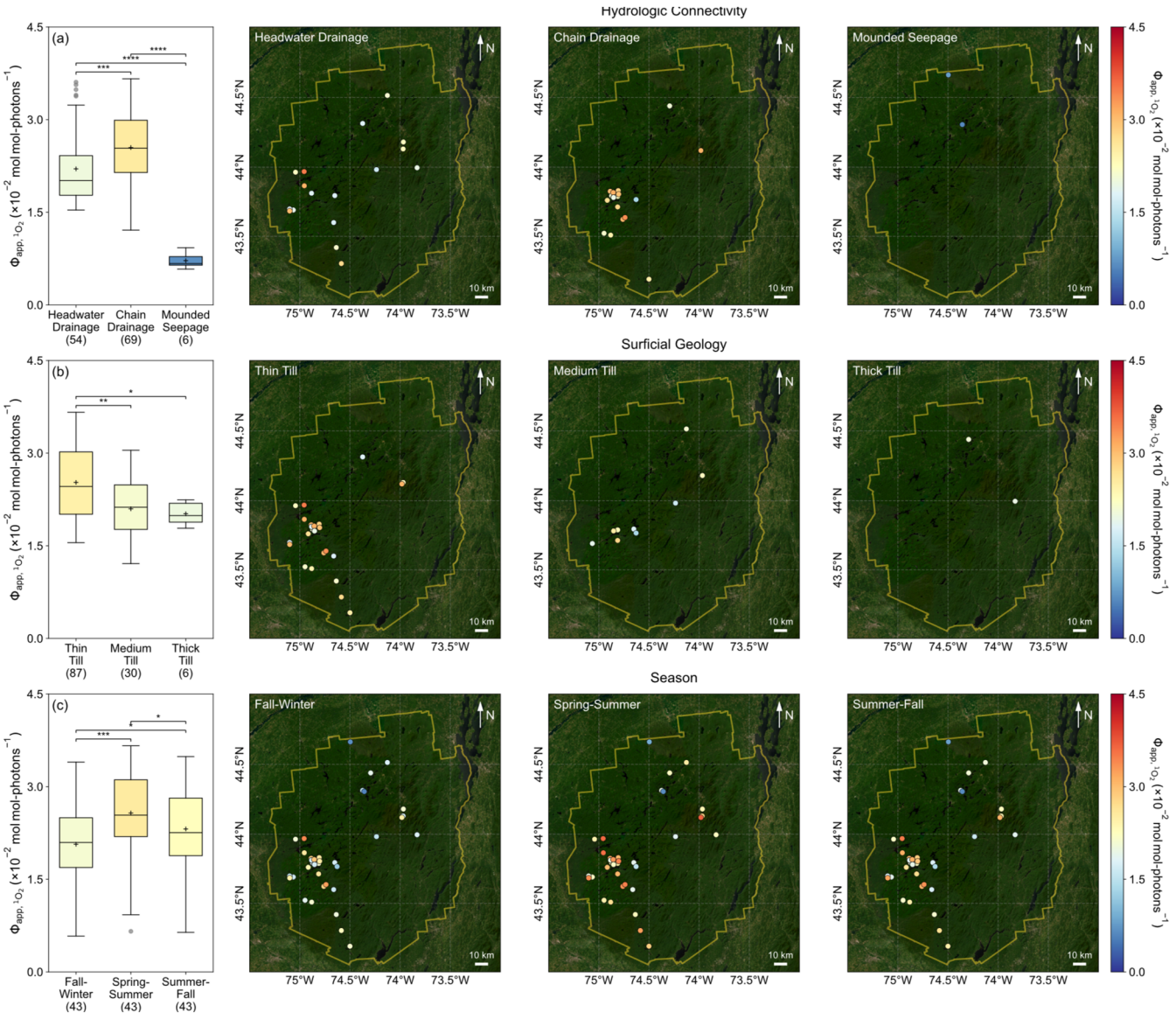

Figure 3. Spatiotemporal patterns of $\Phi_{app,^1O_2}$ for ALTM lakes grouped by (a) hydrologic connectivity (headwater drainage, chain drainage, or mounded seepage), (b) surficial geology (thin till, medium till, or thick till), and (c) season (fall−winter, spring−summer, or summer−fall). On panels (a)−(c), each box spans the 25th to 75th percentiles, with whiskers extending to 1.5 times the interquartile range below the 25th and above the 75th percentiles. The centerline and "+" sign mark the median and mean, respectively. Gray circles represent outliers. Numbers in parentheses represent the number of samples in each group. Box colors correspond to their respective median values referenced against the color bar. For multiple comparisons, a Kruskal−Wallis test was first performed to determine whether statistically significant differences existed among groups. If significant, pairwise Mann−Whitney *U* tests were performed, with significant differences marked by asterisks as "*" ($p < 0.05$), "**" ($p < 0.01$), "***" ($p < 0.001$), or "****" ($p < 0.0001$). On each map, the solid yellow line delineates the boundary of Adirondack Park.

(0.47−3.71; median 1.37; e.g., coastal seawaters in South China[118]). Higher $\Phi_{app,^1O_2}/\Phi^{SRNOM}_{app,^1O_2}$ in these matrices may partly reflect the enhancing effects of halides on FFA reactivity[61] and/or $^1O_2$ production[119] relative to ALTM samples with low specific conductance (14.2 ± 4.6 μS/cm; Table S3). Compared to DOM of other origins, $\Phi_{app,^1O_2}/\Phi^{SRNOM}_{app,^1O_2}$ for ALTM samples were significantly lower than ratios for wastewater samples (0.62−4.97; median 2.26; e.g., effluent organic matter[120]) but showed no statistical difference from those for algal (0.25−3.10; median 1.13), soil (0.48−6.09; median 1.13), or pyrogenic organic matter (0.15−3.04; median 1.27). With normalization to $\Phi^{SRNOM}_{app,^1O_2}$, these semiqualitative comparisons position $\Phi_{app,^1O_2}$ for ALTM samples within the broader literature, though our $\Phi_{app,^1O_2}$ only represent solar-integrated values[48] and bulk aqueous-phase measurements (i.e., that do not account for the microheterogeneous distribution of $^1O_2$[121,122]).

Spatial heterogeneity in $\Phi_{app,^1O_2}$ was evident among lakes with different watershed hydrologic connectivity (Figure 3a) and surficial geology (Figure 3b). $\Phi_{app,^1O_2}$ for headwater and chain drainage lakes ($1.5-3.6 \times 10^{-2}$; median 2.0×10^{-2} and $1.2-3.7 \times 10^{-2}$; median 2.5×10^{-2}) were higher than those for mounded seepage lakes ($0.6-0.9 \times 10^{-2}$; median 0.7×10^{-2}), which is attributable to (1) enhanced $^1O_2$ formation efficiency resulting from DOM with a greater proportion of autochthonous components and smaller molecular sizes in drainage

https://doi.org/10.1021/acs.est.5c04001
Environ. Sci. Technol. XXXX, XXX, XXX−XXX

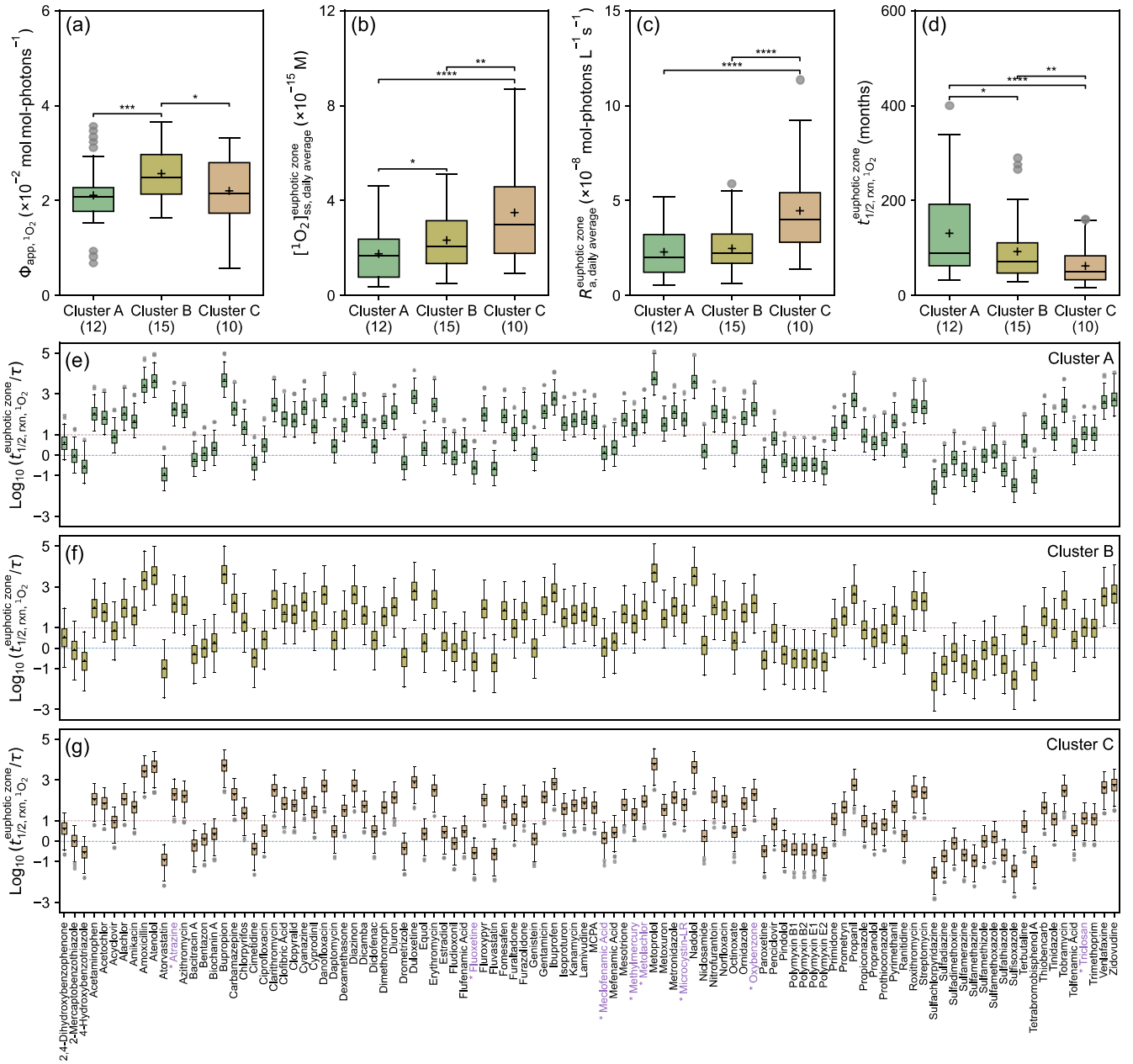

Figure 4. Comparisons of $[^1O_2]_{ss,\ daily\ average}^{euphotic\ zone}$ and the $\log_{10}$-transformed ratios of contaminant half-lives due to reaction with $^1O_2$ in the euphotic zone ($t_{1/2,\ rxn,\ ^1O_2}^{euphotic\ zone}$) to the hydraulic residence times (τ) of ALTM lakes with varying browning status: (a) Multiple comparisons of $\Phi_{app,\ ^1O_2}$ across lake clusters. (b) Multiple comparisons of $[^1O_2]_{ss,\ daily\ average}^{euphotic\ zone}$ across lake clusters. (c) Multiple comparisons of $R_{a,\ daily\ average}^{euphotic\ zone}$ across lake clusters. (d) Multiple comparisons of $t_{1/2,\ rxn,\ ^1O_2}^{euphotic\ zone}$ (estimated based on a median $k_{rxn,\ ^1O_2}$ of 1.8×10^6 M^{-1} s^{-1} for 106 compounds; Table S16) across lake clusters. (e) Cluster-specific distribution of $\log_{10}$-transformed $t_{1/2,\ rxn,\ ^1O_2}^{euphotic\ zone}/\tau$ ratios for 106 compounds in cluster A lakes. (f) Cluster-specific distribution of $\log_{10}$-transformed $t_{1/2,\ rxn,\ ^1O_2}^{euphotic\ zone}/\tau$ ratios for 106 compounds in cluster B lakes. (g) Cluster-specific distribution of $\log_{10}$-transformed $t_{1/2,\ rxn,\ ^1O_2}^{euphotic\ zone}/\tau$ ratios for 106 compounds in cluster C lakes. Lakes in clusters A, B, and C were operationally designated as experiencing mild, moderate, and intense browning, respectively. On panels (a)−(d), each box spans the 25th to 75th percentiles, with whiskers extending to 1.5 times the interquartile range below the 25th and above the 75th percentiles. The centerline and "+" sign mark the median and mean, respectively. Gray circles represent outliers. Numbers in parentheses represent the number of lakes in each cluster. For multiple comparisons, a Kruskal−Wallis test was first performed to determine whether statistically significant differences existed among groups. If significant, pairwise Mann−Whitney *U* tests were performed, with significant differences marked by asterisks as "*" ($p < 0.05$), "**" ($p < 0.01$), "***" ($p < 0.001$), or "****" ($p < 0.0001$). On panels (e) to (g), each box spans the 25th to 75th percentiles, with whiskers extending to 1.5 times the interquartile range below the 25th and above the 75th percentiles. The centerline and "+" sign mark the median and mean, respectively. Gray circles represent outliers. The blue dashed line marks a $t_{1/2,\ rxn,\ ^1O_2}^{euphotic\ zone}/\tau$ ratio of 1, whereas the red dashed line marks a $t_{1/2,\ rxn,\ ^1O_2}^{euphotic\ zone}/\tau$ ratio of 10. Compounds ($n = 8$) highlighted in purple and marked with an asterisk denote those previously detected in Adirondack lake waters.[134−136]

lakes and (2) reduced $^1O_2$ formation efficiency associated with elevated [Fe] in seepage lakes. For example, *E2:E3* (4.14−8.50; median 5.53; Figure S15) and FI (1.36−1.61; median 1.46; Figure S16) of samples from both types of drainage lakes,

https://doi.org/10.1021/acs.est.5c04001
Environ. Sci. Technol. XXXX, XXX, XXX−XXX

which receive most of their water from upland runoff and tributary streams, were higher than those of samples from seepage lakes (4.14−5.14; median 4.59 and 1.28−1.38; median 1.34, respectively) that are sustained mainly by precipitation with minimal upland or groundwater inputs.[51] On the other hand, [Fe] in samples from seepage lakes (13.5−16.7 μM; median 15.6 μM; Figure S17) far exceeded those in samples from drainage lakes (0.3−13.1 μM; median 1.9 μM) and likely exerted a stronger quenching effect on excited states of DOM (e.g., through static and dynamic quenching by bound paramagnetic Fe^{3+}) as demonstrated in titration experiments with humic and fulvic acids or effluent organic matter.[123,124] $\Phi_{app,^1O_2}$ for samples taken from midlake and outlet stream locations at six drainage lakes were not statistically different, possibly due to the relatively short hydraulic residence times of these systems (0.21 ± 0.15 years; Table S1). When further categorized by glacial till depth, $\Phi_{app,^1O_2}$ for thin till drainage lakes ($1.6–3.7 \times 10^{-2}$; median 2.5×10^{-2}) were higher than for both medium till ($1.2–3.1 \times 10^{-2}$; median 2.1×10^{-2}) and thick till ($1.8–2.2 \times 10^{-2}$; median 2.0×10^{-2}) drainage lakes. Such differences in $\Phi_{app,^1O_2}$ may reflect variation in $^1O_2$ formation efficiency from DOM shaped by a dynamic balance between hydrologic inputs from upland runoff with shorter transit times (e.g., delivering DOM that has undergone photochemical and microbial alteration along the terrestrial−aquatic continuum[125,126]) and groundwater inflow with longer residence times (e.g., supplying DOM that is more photodegradable and aerobically biolabile[127]) into lakes underlain by glacial tills of varying depth.[128]

Seasonal variations in $\Phi_{app,^1O_2}$ for ALTM samples followed the pattern of spring−summer > summer−fall > fall−winter (Figure 3c), presumably driven by shifts in the relative contributions of DOM from allochthonous and autochthonous sources (e.g., increased terrestrial inputs during wet periods and elevated phytoplankton production in warmer months), as well as changes in the rates and extent of watershed-scale and in-lake processing of DOM (e.g., enhanced photooxidation under stronger solar irradiance and accelerated microbial reworking at higher temperatures).[108,125] However, previous studies have documented inconsistent seasonal patterns of $\Phi_{app,^1O_2}$ in other surface water systems (e.g., Scandinavian lakes and streams,[116] Lake Superior and its tributaries,[55] and Prairie Pothole wetlands;[109] Figure S20). Throughout the sampling period, the slope of the linear regression between $\Phi_{app,^1O_2}$ and *E2:E3* increased from 0.24 ± 0.08 for fall−winter to 0.57 ± 0.19 for spring−summer and then decreased to 0.28 ± 0.11 for summer−fall (Figure S21). Seasonal slopes for ALTM samples overlapped with those measured for lakes and wetlands in Wisconsin (0.38 ± 0.15; Table S10),[59,110,112] Minnesota (0.22 ± 0.03),[111] and the Prairie Pothole Region (0.62 ± 0.04),[109] as well as with that for Lake Superior (0.19 ± 0.03).[55] Consolidating samples from three seasons into one single data set yielded a slope of 0.21 ± 0.07 and an intercept of 1.1 ± 0.4, which closely matched the global slope (0.26 ± 0.02) and intercept (1.3 ± 0.1) derived from a broader set (n = 1547) of $\Phi_{app,^1O_2}$ ($0.05–18 \times 10^{-2}$; median 2.3×10^{-2}) and *E2:E3* (0.4−29.9; median 5.7). Such convergence should be interpreted with caution, as it does not necessarily imply a generalizable relationship given the substantial variability in slopes and intercepts reported across studies (Table S10).[49,113,129] Though *E2:E3* has long been proposed as a predictor of $\Phi_{app,^1O_2}$,[114] generalized additive modeling (which uses penalized regression splines to model both linear and nonlinear relationships among multiple factors[130]) identified $S_{290–400}$ and FI as linear predictors and [Fe] as a nonlinear predictor of $\Phi_{app,^1O_2}$ for ALTM samples across seasons (Figures S24−S26). Slopes from the linear regression between $\Phi_{app,^1O_2}$ and $S_{290–400}$ followed a similar pattern to those of *E2:E3*, with the steepest slope observed during spring−summer (Figure S22). Spectral slope coefficients such as $S_{290–400}$[131,132] and $S_{300–600}$[55,113,117] are indicators of DOM processing and have therefore been explored as alternative single predictors of $\Phi_{app,^1O_2}$ to *E2:E3*. Slopes from the linear regression between $\Phi_{app,^1O_2}$ and FI, in contrast, remained relatively stable (6.6 ± 1.4 for fall−winter, 6.7 ± 1.5 for spring−summer, and 6.8 ± 1.3 for summer−fall; Figure S23). Complementary to $S_{290–400}$ and FI, [Fe] exerted a nonlinear negative influence on $\Phi_{app,^1O_2}$, which qualitatively aligned with the bivariate patterns identified by Spearman's correlation analysis (Figure S27). Taken together, these analyses highlight the interplay between hydrogeological conditions and DOM quality in shaping the spatiotemporal patterns of $\Phi_{app,^1O_2}$ for ALTM lakes.

$^1O_2$ Production in Relation to Lake Browning. Overall, $\Phi_{app,^1O_2}$ for samples from ALTM lakes experiencing mild (i.e., cluster A) or intense browning (i.e., cluster C) were lower than those for samples from lakes undergoing moderate browning (i.e., cluster B; Figure 4a). Cluster A samples were characterized by the highest pH (which favors deactivation of excited states of DOM based on the charge-transfer model[133]) and the lowest FI (suggesting limited contribution from autochthonous DOM[56]), along with comparatively high E2:E3 (which reduces the probability of charge-transfer interactions[114]) and low [Fe] (indicating weak quenching of excited states of DOM by Fe^{3+};[124] Figures S28 and S29). Cluster C samples exhibited lower pH and *E2:E3* but higher FI and [Fe] than cluster A samples; however, $\Phi_{app,^1O_2}$ for samples from these two clusters of lakes showed no significant difference. Cluster B samples struck a balance among these factors, with moderate pH (lower than cluster A but higher than cluster C), high *E2:E3* (similar to cluster A but higher than cluster C), high FI (similar to cluster C but higher than cluster A), and low [Fe] (similar to cluster A but lower than cluster C), again illustrating the multifaceted and sometimes contrasting effects of the water chemistry and DOM composition on $\Phi_{app,^1O_2}$.

To estimate steady-state concentrations of $^1O_2$ in ALTM lakes, depth-averaged values such as $[^1O_2]^{\text{euphotic zone}}_{\text{ss, daily average}}$ and $[^1O_2]^{\text{epilimnion}}_{\text{ss, daily average}}$ were calculated in light of their relevance for photochemical modeling.[48] $[^1O_2]^{\text{euphotic zone}}_{\text{ss, daily average}}$ ranged from 3.6×10^{-16} to 9.3×10^{-15} M (Table S13), whereas $[^1O_2]^{\text{epilimnion}}_{\text{ss, daily average}}$ ranged from 5.7×10^{-16} to 1.7×10^{-14} M (Table S14), which fell on the upper end of the depth-averaged concentrations predicted for lake epilimnia globally (e.g., $6 \times 10^{-17}–5 \times 10^{-15}$ M).[48] On average, the ratio of $[^1O_2]^{\text{epilimnion}}_{\text{ss, daily average}}$ to $[^1O_2]^{\text{euphotic zone}}_{\text{ss, daily average}}$ was 1.8 ± 0.7, but $[^1O_2]^{\text{epilimnion}}_{\text{ss, daily average}}$ were excluded from further analysis because epilimnion depths were derived from static lake surface areas[137] rather than predicted as a function of DOC (as was done for euphotic zone depths[72]). $[^1O_2]^{\text{euphotic zone}}_{\text{ss, daily average}}$ were 7 ± 2% of $[^1O_2]^{\text{near-surface}}_{\text{ss, daily average}}$ (4.8×10^{-15} to 1.3×10^{-13} M; Table S15), which concurred with earlier findings that depth-

https://doi.org/10.1021/acs.est.5c04001
Environ. Sci. Technol. XXXX, XXX, XXX−XXX

averaged $[^1O_2]_{ss}$ are 1−2 orders of magnitude lower than near-surface $[^1O_2]_{ss}$ because of light attenuation within the water column (Figures S30−S32).[48] Compared to $\Phi_{app,^1O_2}$, $[^1O_2]^{euphotic\ zone}_{ss,\ daily\ average}$ were less influenced by watershed hydrologic connectivity and surficial geology but followed a similar seasonal pattern of spring−summer > summer−fall > fall−winter (Figure S33). Consistently across seasons, $[^1O_2]^{euphotic\ zone}_{ss,\ daily\ average}$ were highest in cluster C lakes and lowest in cluster A lakes (Figure S34), although $\Phi_{app,^1O_2}$ were not statistically different across lake clusters within the same season (Figure S35). Considering the similarity in water temperature, dissolved oxygen, and specific conductance among lake clusters (Figure S28), the elevated $[^1O_2]^{euphotic\ zone}_{ss,\ daily\ average}$ in cluster C lakes (Figure 4b) were largely driven by higher volumetric light absorption rates (Figure 4c), which outweighed the influence of $\Phi_{app,^1O_2}$ when compared with clusters A and B lakes characterized by deeper euphotic zones. $[^1O_2]^{euphotic\ zone}_{ss,\ daily\ average}$ in cluster B lakes exceeded those in cluster A lakes, as expected from their comparable volumetric light absorption rates and the higher $\Phi_{app,^1O_2}$ for cluster B samples.

Continued browning has been projected to enhance $^1O_2$ formation and accelerate $^1O_2$-mediated reactions in sunlit lakes.[24] Of the ALTM lakes surveyed in this work, 12 were also sampled once in 2018 for photochemical characterization.[131] $[^1O_2]^{euphotic\ zone}_{ss,\ daily\ average}$ in this subset of lakes were higher in 2023 than in 2018 across clusters (Figure S34) despite no significant difference in $\Phi_{app,^1O_2}$ for samples collected in these two years (Figure S35). Generalizing $^1O_2$ production in response to browning was not possible with such limited temporal data. To partially address this constraint, a space-for-time substitution approach[138] was applied to $[^1O_2]^{euphotic\ zone}_{ss,\ daily\ average}$ estimated for 1469 Adirondack lakes with historical water chemistry data.[16,30] $[^1O_2]^{euphotic\ zone}_{ss,\ daily\ average}$ (1.1×10^{-15}–2.3×10^{-14} M; median 4.4×10^{-15} M) in this broader set of lakes showed strong positive correlations with both DOC and color (Figure S36), consistent with the relationships simulated for boreal lakes across Sweden.[25] Should DOC and color continue to rise, $[^1O_2]^{euphotic\ zone}_{ss,\ daily\ average}$ are expected to increase; however, the degree to which spatial patterns can substitute for temporal trends warrants validation,[139] as our estimates relied on a small photochemical data set relative to the spatiotemporal scale of interest.

To assess the significance of $^1O_2$ in regulating contaminant dynamics in ALTM lakes, biomolecular and/or total quenching rate constants for its reactions with a variety of compounds (e.g., amino acids, peptides, pesticides, pharmaceuticals, phytoestrogens) were compiled from 66 references (Table S17). For these compounds, biomolecular reaction rate constants ($k_{rxn,\ ^1O_2}$) measured under environmentally relevant conditions (i.e., in aqueous solutions between 5 and 9 using competition kinetics or kinetic solvent isotope effect methods) spanned over five orders of magnitude, ranging from 6.3×10^3 to 3.7×10^9 M^{-1} s^{-1} with a median of 1.3×10^7 M^{-1} s^{-1} (n = 192). Given the mildly acidic to neutral pH of ALTM samples (i.e., 6.02 ± 0.64; Table S3), a subset of 106 anthropogenic contaminants and natural toxins with $k_{rxn,\ ^1O_2}$ measured under similar pH conditions (Table S16) was prioritized to further evaluate their $^1O_2$-mediated half-lives in the euphotic zone ($t^{euphotic\ zone}_{1/2,\ rxn,\ ^1O_2}$; Figure S37). Eight of these 106 compounds, including six organic micropollutants (i.e., atrazine, fluoxetine, meclofenamic acid, metolachlor, oxybenzone, triclosan),[134] methylmercury,[135] and microcystin-LR,[136] have been previously detected in Adirondack lakes. With a median $k_{rxn,\ ^1O_2}$ of 1.8×10^6 M^{-1} s^{-1} (based on data for 106 compounds), half-lives due to reaction with $^1O_2$ were estimated to range from 32 to 400 months in the euphotic zone of cluster A lakes, 29 to 290 months in cluster B lakes, and 17 to 160 months in cluster C lakes (Figure 4d). Comparing the $\log_{10}$-transformed ratios of $t^{euphotic\ zone}_{1/2,\ rxn,\ ^1O_2}$ to the hydraulic residence times (τ) of ALTM lakes (Figure 4e−g) revealed that 47 of the 106 compounds yielded mean ratios below 0 (e.g., sulfonamide antibiotics,[41] antimicrobial peptides,[44] benzotriazole derivatives[38,42]) or between 0 and 1 (e.g., fenamates,[40] antiherpesvirus agents,[39] isoflavone phytoestrogens[43]), suggesting that $^1O_2$-mediated reactions occur on time scales shorter than or comparable to lake flushing. For the remaining compounds with mean ratios exceeding 1, $^1O_2$-mediated reactions are unlikely to govern their fate, but natural attenuation in ALTM lakes may still proceed via pathways involving other reactive intermediates and/or nonphotolytic transformation or partitioning processes.

■ ENVIRONMENTAL IMPLICATIONS

Our work integrated time series and trend analyses of long-term monitoring data sets with photochemical characterization of field samples to investigate $^1O_2$ production in ALTM lakes, which complements prior modeling studies that predicted the effects of browning on the photochemical production of reactive intermediates in sunlit surface waters.[25−28] Through wavelet coherence analysis, we identified recovery from acid deposition and changes in precipitation as potential drivers of DOC dynamics in ALTM lakes over longer time scales, while solar irradiance and soil wetness emerged as additional contributors at shorter time scales. Classifying browning status based on Sen's slopes of temporal trends enabled us to perform a comparative analysis of $^1O_2$ formation among ALTM lakes, although the broader applicability of this framework warrants further evaluation, as the extent and drivers of lake browning may vary across geographic regions[13] or shift with the temporal window of analysis.[140] Our study was somewhat limited in terms of photochemical data, as it focused only on $^1O_2$. Even so, the depth-averaged steady-state concentrations of other reactive intermediates, such as ^{3}DOM* (e.g., 10^{-16}–10^{-15} M) and $^\bullet$OH (e.g., 10^{-18}–10^{-17} M), in the euphotic zone of ALTM lakes can be approximated through their known orders of magnitude relative to $[^1O_2]_{ss}$.[48,141] Lakes experiencing more intense browning exhibit higher $[^1O_2]_{ss}$; however, whether the concentration patterns of ^{3}DOM* and $^\bullet$OH track with or diverge from that of $^1O_2$ across the browning gradient requires additional photochemical measurements and careful consideration of uncertainties (e.g., the bimolecular reaction rate constants of probes with ^{3}DOM*[141] and the specificity of probes in distinguishing $^\bullet$OH from lower-energy hydroxylating species[142]). Concurrent with browning, warming of lake surface waters[16] also alters nutrient availability, light regimes, and thermal conditions,[16,128,139] which may further complicate predictions of $^1O_2$ production due to cascading effects on DOM properties[17] and pathways involved in $^1O_2$ formation and quenching.[49] Overall, this study serves as a springboard for further research into the impact of browning on photochemistry in Adirondack lakes and similar aquatic systems and underscores the need for long-term monitoring of DOM quality and photochemical parameters to better understand

https://doi.org/10.1021/acs.est.5c04001
Environ. Sci. Technol. XXXX, XXX, XXX−XXX

their implications for ecosystem function and water quality management.

■ ASSOCIATED CONTENT

Supporting Information

The Supporting Information is available free of charge at https://pubs.acs.org/doi/10.1021/acs.est.5c04001.

Map, morphometric characteristics, and watershed attributes of Adirondack Long-Term Monitoring (ALTM) lakes. Water chemistry parameters and optical properties of ALTM samples. Photochemistry experimental details and summary of photochemical parameters. Wavelet coherence tests between the time series of DOC and external drivers. Sen's slopes for the time series of DOC, color, and $SUVA_{254}$. Comparisons of $\Phi_{app,^1O_2}$ for ALTM samples with literature data. Linear regression between $\Phi_{app,^1O_2}$ and selected optical properties. Generalized additive modeling of seasonal variations in $\Phi_{app,^1O_2}$. Steady-state concentrations and depth profiles of $^1O_2$ in the euphotic zone of ALTM lakes. Half-lives of selected contaminants in the euphotic zone due to reaction with $^1O_2$. Summary of literature data on $k_{rxn,^1O_2}$ and $\Phi_{app,^1O_2}$.(PDF)

■ AUTHOR INFORMATION

Corresponding Author

Teng Zeng − *Department of Civil and Environmental Engineering, Syracuse University, Syracuse, New York 13244, United States;* orcid.org/0000-0002-0374-9549; Phone: +1-315-443-1099; Email: tezeng@syr.edu

Authors

Birdem Öz − *Department of Civil and Environmental Engineering, Syracuse University, Syracuse, New York 13244, United States;* Present Address: JKMuir, LLC, 2275 Silas Deane Highway, Rocky Hill, Connecticut 06067, United States

Philip K. Snyder − *Ausable Freshwater Center, Wilmington, New York 12997, United States*

Xiaoyu Jiao − *Department of Civil and Environmental Engineering, Syracuse University, Syracuse, New York 13244, United States*

Charles T. Driscoll − *Department of Civil and Environmental Engineering, Syracuse University, Syracuse, New York 13244, United States;* orcid.org/0000-0003-2692-2890

Complete contact information is available at: https://pubs.acs.org/10.1021/acs.est.5c04001

Notes

The authors declare no competing financial interest.

■ ACKNOWLEDGMENTS

We gratefully acknowledge Dr. Christian A. Gueymard (Solar Consulting Services) for providing access to *SMARTS v2.9.9*, as well as Tricia A. Lincoln and Michael R. McHale (U.S. Geological Survey) for sharing water chemistry data. We further thank the editor and anonymous reviewers for their constructive feedback. This work was supported by the New York State Energy Research and Development Authority (NYSERDA) under Award No. 216244 and by the New York State Department of Environmental Conservation (NYSDEC) through the Ausable Freshwater Center under Award No. 2023-DEC/SCALE #1:4. This material is based upon work supported by the National Science Foundation under Grant No. 2145214.

■ REFERENCES

(1) Monteith, D. T.; Stoddard, J. L.; Evans, C. D.; de Wit, H. A.; Forsius, M.; Høgåsen, T.; Wilander, A.; Skjelkvåle, B. L.; Jeffries, D. S.; Vuorenmaa, J.; Keller, B.; Kopácek, J.; Vesely, J. Dissolved organic carbon trends resulting from changes in atmospheric deposition chemistry. *Nature* **2007**, *450*, 537−540.

(2) de Wit, H. A.; Stoddard, J. L.; Monteith, D. T.; Sample, J. E.; Austnes, K.; Couture, S.; Fölster, J.; Higgins, S. N.; Houle, D.; Hruška, J.; Krám, P.; Kopáček, J.; Paterson, A. M.; Valinia, S.; Van Dam, H.; Vuorenmaa, J.; Evans, C. D. Cleaner air reveals growing influence of climate on dissolved organic carbon trends in northern headwaters. *Environ. Res. Lett.* **2021**, *16* (10), No. 104009.

(3) Blanchet, C. C.; Arzel, C.; Davranche, A.; Kahilainen, K. K.; Secondi, J.; Taipale, S.; Lindberg, H.; Loehr, J.; Manninen-Johansen, S.; Sundell, J.; Maanan, M.; Nummi, P. Ecology and extent of freshwater browning - What we know and what should be studied next in the context of global change. *Sci. Total Environ.* **2022**, *812*, No. 152420.

(4) Battarbee, R. W.; Shilland, E. M.; Kernan, M.; Monteith, D. T.; Curtis, C. J. Recovery of acidified surface waters from acidification in the United Kingdom after twenty years of chemical and biological monitoring (1988−2008). *Ecol. Indic.* **2014**, *37*, 267−273.

(5) Driscoll, C. T.; Driscoll, K. M.; Fakhraei, H.; Civerolo, K. Long-term temporal trends and spatial patterns in the acid-base chemistry of lakes in the Adirondack region of New York in response to decreases in acidic deposition. *Atmos. Environ.* **2016**, *146* (Supplement C), 5−14.

(6) Imtiazy, M. N.; Paterson, A. M.; Higgins, S. N.; Yao, H.; Couture, S.; Hudson, J. J. Dissolved organic carbon in eastern Canadian lakes: Novel patterns and relationships with regional and global factors. *Sci. Total Environ.* **2020**, *726*, No. 138400.

(7) de Wit, H. A.; Valinia, S.; Weyhenmeyer, G. A.; Futter, M. N.; Kortelainen, P.; Austnes, K.; Hessen, D. O.; Räike, A.; Laudon, H.; Vuorenmaa, J. Current browning of surface waters will be further promoted by wetter climate. *Environ. Sci. Technol. Lett.* **2016**, *3* (12), 430−435.

(8) Strock, K. E.; Saros, J. E.; Nelson, S. J.; Birkel, S. D.; Kahl, J. S.; McDowell, W. H. Extreme weather years drive episodic changes in lake chemistry: Implications for recovery from sulfate deposition and long-term trends in dissolved organic carbon. *Biogeochemistry* **2016**, *127* (2), 353−365.

(9) Weyhenmeyer, G. A.; Karlsson, J. Nonlinear response of dissolved organic carbon concentrations in boreal lakes to increasing temperatures. *Limnol. Oceanogr.* **2009**, *54* (6, Part 2), 2513−2519.

(10) Finstad, A. G.; Andersen, T.; Larsen, S.; Tominaga, K.; Blumentrath, S.; de Wit, H. A.; Tømmervik, H.; Hessen, D. O. From greening to browning: Catchment vegetation development and reduced S-deposition promote organic carbon load on decadal time scales in Nordic lakes. *Sci. Rep.* **2016**, *6* (1), No. 31944.

(11) Kritzberg, E. S. Centennial-long trends of lake browning show major effect of afforestation. *Limnol. Oceanogr. Lett.* **2017**, *2* (4), 105−112.

(12) Estlander, S.; Pippingsköld, E.; Horppila, J. Artificial ditching of catchments and brownification-connected water quality parameters of lakes. *Water Res.* **2021**, *205*, No. 117674.

(13) Lapierre, J.-F.; Collins, S. M.; Oliver, S. K.; Stanley, E. H.; Wagner, T. Inconsistent browning of northeastern U.S. lakes despite increased precipitation and recovery from acidification. *Ecosphere* **2021**, *12* (3), No. e03415.

(14) Rodríguez-Cardona, B. M.; Houle, D.; Couture, S.; Lapierre, J.-F.; del Giorgio, P. A. Long-term trends in carbon and color signal uneven browning and terrestrialization of northern lakes. *Commun. Earth Environ.* **2023**, *4* (1), No. 338.

(15) Isles, P. D. F.; Creed, I. F.; Jonsson, A.; Bergström, A.-K. Trade-offs between light and nutrient availability across gradients of dissolved organic carbon lead to spatially and temporally variable responses of lake phytoplankton biomass to browning. *Ecosystems* **2021**, *24* (8), 1837−1852.
(16) Jane, S. F.; Detmer, T. M.; Larrick, S. L.; Rose, K. C.; Randall, E. A.; Jirka, K. J.; McIntyre, P. B. Concurrent warming and browning eliminate cold-water fish habitat in many temperate lakes. *Proc. Natl. Acad. Sci. U.S.A.* **2024**, *121* (2), No. e2306906120.
(17) Creed, I. F.; Bergström, A.-K.; Trick, C. G.; Grimm, N. B.; Hessen, D. O.; Karlsson, J.; Kidd, K. A.; Kritzberg, E.; McKnight, D. M.; Freeman, E. C.; Senar, O. E.; Andersson, A.; Ask, J.; Berggren, M.; Cherif, M.; Giesler, R.; Hotchkiss, E. R.; Kortelainen, P.; Palta, M. M.; Vrede, T.; Weyhenmeyer, G. A. Global change-driven effects on dissolved organic matter composition: Implications for food webs of northern lakes. *Global Change Biol.* **2018**, *24* (8), 3692−3714.
(18) Kritzberg, E. S.; Hasselquist, E. M.; Škerlep, M.; Löfgren, S.; Olsson, O.; Stadmark, J.; Valinia, S.; Hansson, L.-A.; Laudon, H. Browning of freshwaters: Consequences to ecosystem services, underlying drivers, and potential mitigation measures. *Ambio* **2020**, *49* (2), 375−390.
(19) Eikebrokk, B.; Vogt, R. D.; Liltved, H. NOM increase in Northern European source waters: Discussion of possible causes and impacts on coagulation/contact filtration processes. *Water Supply* **2004**, *4* (4), 47−54.
(20) Keucken, A.; Heinicke, G.; Persson, K.; Köhler, S. Combined coagulation and ultrafiltration process to counteract increasing NOM in brown surface water. *Water* **2017**, *9* (9), No. 697.
(21) Anderson, L. E.; Krkošek, W. H.; Stoddart, A. K.; Trueman, B. F.; Gagnon, G. A. Lake recovery through reduced sulfate deposition: A new paradigm for drinking water treatment. *Environ. Sci. Technol.* **2017**, *51* (3), 1414−1422.
(22) Anderson, L. E.; DeMont, I.; Dunnington, D. D.; Bjorndahl, P.; Redden, D. J.; Brophy, M. J.; Gagnon, G. A. A review of long-term change in surface water natural organic matter concentration in the northern hemisphere and the implications for drinking water treatment. *Sci. Total Environ.* **2023**, *858*, No. 159699.
(23) Swinamer, R.; Anderson, L. E.; Redden, D.; Bjorndahl, P.; Campbell, J.; Krkošek, W. H.; Gagnon, G. A. Climate-driven increases in source water natural organic matter: Implications for the sustainability of drinking water treatment. *Environ. Sci. Technol.* **2024**, *58* (27), 11958−11969.
(24) Vione, D.; Scozzaro, A. Photochemistry of surface fresh waters in the framework of climate change. *Environ. Sci. Technol.* **2019**, *53* (14), 7945−7963.
(25) Koehler, B.; Barsotti, F.; Minella, M.; Landelius, T.; Minero, C.; Tranvik, L. J.; Vione, D. Simulation of photoreactive transients and of photochemical transformation of organic pollutants in sunlit boreal lakes across 14 degrees of latitude: A photochemical mapping of Sweden. *Water Res.* **2018**, *129*, 94−104.
(26) Wolf, R.; Thrane, J.-E.; Hessen, D. O.; Andersen, T. Modelling ROS formation in boreal lakes from interactions between dissolved organic matter and absorbed solar photon flux. *Water Res.* **2018**, *132*, 331−339.
(27) Calderaro, F.; Vione, D. Possible effect of climate change on surface-water photochemistry: A model assessment of the impact of browning on the photodegradation of pollutants in lakes during summer stratification. Epilimnion vs. whole-lake phototransformation. *Molecules* **2020**, *25* (12), No. 2795.
(28) Vione, D.; Rosario-Ortiz, F. L. Foreseen effects of climate-impacted scenarios on the photochemical fate of selected cyanotoxins in surface freshwaters. *Environ. Sci. Technol.* **2021**, *55* (16), 10928−10934.
(29) Adirondack Lakes Survey Corporation and New York State Department of Environmental Conservation. *The Adirondack Long-Term Monitoring Lakes: A Compendium of Site Descriptions, Recent Chemistry and Selected Research Information*; The New York State Energy Research and Development Authority: Albany, NY, 2019; pp 1−335.
(30) Kretzer, W.; Roy, K.; Dukett, J.; Houck, N.; Philip, S. Adirondack Lakes Survey 1984−1987 Complete Data Set, 2023.
(31) Weishaar, J. L.; Aiken, G. R.; Bergamaschi, B. A.; Fram, M. S.; Fujii, R.; Mopper, K. Evaluation of specific ultraviolet absorbance as an indicator of the chemical composition and reactivity of dissolved organic carbon. *Environ. Sci. Technol.* **2003**, *37* (20), 4702−4708.
(32) Cory, R. M.; Cotner, J. B.; McNeill, K. Quantifying interactions between singlet oxygen and aquatic fulvic acids. *Environ. Sci. Technol.* **2009**, *43* (3), 718−723.
(33) Boreen, A. L.; Edhlund, B. L.; Cotner, J. B.; McNeill, K. Indirect photodegradation of dissolved free amino acids: The contribution of singlet oxygen and the differential reactivity of DOM from various sources. *Environ. Sci. Technol.* **2008**, *42* (15), 5492−5498.
(34) Cory, R. M.; McNeill, K.; Cotner, J. P.; Amado, A.; Purcell, J. M.; Marshall, A. G. Singlet oxygen in the coupled photochemical and biochemical oxidation of dissolved organic matter. *Environ. Sci. Technol.* **2010**, *44* (10), 3683−3689.
(35) Glaeser, S. P.; Grossart, H.-P.; Glaeser, J. Singlet oxygen, a neglected but important environmental factor: Short-term and long-term effects on bacterioplankton composition in a humic lake. *Environ. Microbiol.* **2010**, *12* (12), 3124−3136.
(36) Waggoner, D. C.; Wozniak, A. S.; Cory, R. M.; Hatcher, P. G. The role of reactive oxygen species in the degradation of lignin derived dissolved organic matter. *Geochim. Cosmochim. Acta* **2017**, *208*, 171−184.
(37) Latch, D. E.; Stender, B. L.; Packer, J. L.; Arnold, W. A.; McNeill, K. Photochemical fate of pharmaceuticals in the environment: Cimetidine and ranitidine. *Environ. Sci. Technol.* **2003**, *37* (15), 3342−3350.
(38) Janssen, E. M. L.; Marron, E.; McNeill, K. Aquatic photochemical kinetics of benzotriazole and structurally related compounds. *Environ. Sci.: Processes Impacts* **2015**, *17* (5), 939−946.
(39) An, J.; Li, G.; An, T.; Nie, X. Indirect photochemical transformations of acyclovir and penciclovir in aquatic environments increase ecological risk. *Environ. Toxicol. Chem.* **2015**, *35* (3), 584−592.
(40) Davis, C. A.; Erickson, P. R.; McNeill, K.; Janssen, E. M. L. Environmental photochemistry of fenamate NSAIDs and their radical intermediates. *Environ. Sci.: Processes Impacts* **2017**, *19* (5), 656−665.
(41) Ge, L.; Zhang, P.; Halsall, C.; Li, Y.; Chen, C.-E.; Li, J.; Sun, H.; Yao, Z. The importance of reactive oxygen species on the aqueous phototransformation of sulfonamide antibiotics: Kinetics, pathways, and comparisons with direct photolysis. *Water Res.* **2019**, *149*, 243−250.
(42) Chen, X.; Wang, J.; Chen, J.; Zhou, C.; Cui, F.; Sun, G. Photodegradation of 2-(2-hydroxy-5-methylphenyl)benzotriazole (UV-P) in coastal seawaters: Important role of DOM. *J. Environ. Sci.* **2019**, *85*, 129−137.
(43) Felcyn, J. R.; Davis, J. C. C.; Tran, L. H.; Berude, J. C.; Latch, D. E. Aquatic photochemistry of isoflavone phytoestrogens: Degradation kinetics and pathways. *Environ. Sci. Technol.* **2012**, *46* (12), 6698−6704.
(44) Davis, C. A.; Janssen, E. M. L. Environmental fate processes of antimicrobial peptides daptomycin, bacitracins, and polymyxins. *Environ. Int.* **2020**, *134*, No. 105271.
(45) Kohn, T.; Nelson, K. L. Sunlight-mediated inactivation of MS2 coliphage via exogenous singlet oxygen produced by sensitizers in natural waters. *Environ. Sci. Technol.* **2007**, *41* (1), 192−197.
(46) Remucal, C. K.; McNeill, K. Photosensitized amino acid degradation in the presence of riboflavin and its derivatives. *Environ. Sci. Technol.* **2011**, *45* (12), 5230−5237.
(47) Rosado-Lausell, S. L.; Wang, H.; Gutiérrez, L.; Romero-Maraccini, O. C.; Niu, X.-Z.; Gin, K. Y. H.; Croué, J.-P.; Nguyen, T. H. Roles of singlet oxygen and triplet excited state of dissolved organic matter formed by different organic matters in bacteriophage MS2 inactivation. *Water Res.* **2013**, *47* (14), 4869−4879.

https://doi.org/10.1021/acs.est.5c04001
Environ. Sci. Technol. XXXX, XXX, XXX−XXX

(48) Partanen, S. B.; Apell, J. N.; Lin, J.; McNeill, K. Factors affecting the mixed-layer concentrations of singlet oxygen in sunlit lakes. *Environ. Sci.: Processes Impacts* **2021**, *23* (8), 1130−1145.
(49) Ossola, R.; Jönsson, O. M.; Moor, K.; McNeill, K. Singlet oxygen quantum yields in environmental waters. *Chem. Rev.* **2021**, *121* (7), 4100−4146.
(50) *Adirondack Long-Term Lakes Monitoring (ALTM)* U.S. Geological Survey New York Water Science Center: Troy, NY; 2023.
(51) Newton, R. M.; Driscoll, C. T. Classification of ALSC Lakes. In *Adirondack Lakes Survey: An Interpretive Analysis of Fish Communities and Water Chemistry, 1984−1987*; Baker, J. P.; Gherini, S. A.; Christensen, S. W.; Driscoll, C. T.; Gallagher, J.; Munson, R. K.; Newton, R. M.; Reckhow, K. H.; Schofield, C. L., Eds.; Adirondack Lakes Survey Corporation: Ray Brook, NY, 1990; pp 2−70.
(52) Cuthbert, I. D.; del Giorgio, P. Toward a standard method of measuring color in freshwater. *Limnol. Oceanogr.* **1992**, *37* (6), 1319−1326.
(53) De Haan, H.; De Boer, T. Applicability of light absorbance and fluorescence as measures of concentration and molecular size of dissolved organic carbon in humic Lake Tjeukemeer. *Water Res.* **1987**, *21* (6), 731−734.
(54) Moran, M. A.; Sheldon, W. M., Jr.; Zepp, R. G. Carbon loss and optical property changes during long-term photochemical and biological degradation of estuarine dissolved organic matter. *Limnol. Oceanogr.* **2000**, *45* (6), 1254−1264.
(55) Peterson, B. M.; McNally, A. M.; Cory, R. M.; Thoemke, J. D.; Cotner, J. B.; McNeill, K. Spatial and temporal distribution of singlet oxygen in Lake Superior. *Environ. Sci. Technol.* **2012**, *46* (13), 7222−7229.
(56) McKnight, D. M.; Boyer, E. W.; Westerhoff, P. K.; Doran, P. T.; Kulbe, T.; Andersen, D. T. Spectrofluorometric characterization of dissolved organic matter for indication of precursor organic material and aromaticity. *Limnol. Oceanogr.* **2001**, *46* (1), 38−48.
(57) Zsolnay, A.; Baigar, E.; Jimenez, M.; Steinweg, B.; Saccomandi, F. Differentiating with fluorescence spectroscopy the sources of dissolved organic matter in soils subjected to drying. *Chemosphere* **1999**, *38* (1), 45−50.
(58) Wilson, H. F.; Xenopoulos, M. A. Effects of agricultural land use on the composition of fluvial dissolved organic matter. *Nat. Geosci.* **2009**, *2*, 37−41.
(59) Maizel, A. C.; Remucal, C. K. The effect of probe choice and solution conditions on the apparent photoreactivity of dissolved organic matter. *Environ. Sci.: Processes Impacts* **2017**, *19* (8), 1040−1050.
(60) Haag, W. R.; Hoigné, J.; Gassman, E.; Braun, A. M. Singlet oxygen in surface waters - Part I: Furfuryl alcohol as a trapping agent. *Chemosphere* **1984**, *13* (5−6), 631−640.
(61) Appiani, E.; Ossola, R.; Latch, D. E.; Erickson, P. R.; McNeill, K. Aqueous singlet oxygen reaction kinetics of furfuryl alcohol: Effect of temperature, pH, and salt content. *Environ. Sci.: Processes Impacts* **2017**, *19* (4), 507−516.
(62) Mostafa, S.; Rosario-Ortiz, F. L. Singlet oxygen formation from wastewater organic matter. *Environ. Sci. Technol.* **2013**, *47* (15), 8179−8186.
(63) Leifer, A. *The Kinetics of Environmental Aquatic Photochemistry: Theory and Practice*; American Chemical Society: Washington, D.C., 1988.
(64) Laszakovits, J. R.; Berg, S. M.; Anderson, B. G.; O'Brien, J. E.; Wammer, K. H.; Sharpless, C. M. *p*-Nitroanisole/pyridine and *p*-nitroacetophenone/pyridine actinometers revisited: Quantum yield in comparison to ferrioxalate. *Environ. Sci. Technol. Lett.* **2017**, *4* (1), 11−14.
(65) Apell, J. N.; McNeill, K. Updated and validated solar irradiance reference spectra for estimating environmental photodegradation rates. *Environ. Sci.: Processes Impacts* **2019**, *21* (3), 427−437.
(66) Partanen, S. B.; McNeill, K. Global corrections to reference irradiance spectra for non-clear-sky conditions. *Environ. Sci. Technol.* **2023**, *57* (6), 2682−2690.
(67) Gueymard, C. A. SMARTS2, A Simple Model of the Atmospheric Radiative Transfer of Sunshine: Algorithms and Performance Assessment, Thesis; Florida Solar Energy Center/University of Central Florida: Cocoa, FL, 1995.
(68) Gueymard, C. A. Parameterized transmittance model for direct beam and circumsolar spectral irradiance. *Sol. Energy* **2001**, *71* (5), 325−346.
(69) Gueymard, C. A. The SMARTS spectral irradiance model after 25 years: New developments and validation of reference spectra. *Sol. Energy* **2019**, *187*, 233−253.
(70) Zepp, R. G.; Cline, D. M. Rates of direct photolysis in aquatic environment. *Environ. Sci. Technol.* **1977**, *11* (4), 359−366.
(71) Bukaveckas, P. A.; Robbins-Forbes, M. Role of dissolved organic carbon in the attenuation of photosynthetically active and ultraviolet radiation in Adirondack lakes. *Freshw. Biol.* **2000**, *43* (3), 339−354.
(72) Morris, D. P.; Zagarese, H.; Williamson, C. E.; Balseiro, E. G.; Hargreaves, B. R.; Modenutti, B.; Moeller, R.; Queimalinos, C. The attenuation of solar UV radiation in lakes and the role of dissolved organic carbon. *Limnol. Oceanogr.* **1995**, *40* (8), 1381−1391.
(73) Zuur, A. F.; Ieno, E. N.; Elphick, C. S. A protocol for data exploration to avoid common statistical problems. *Methods Ecol. Evol.* **2010**, *1* (1), 3−14.
(74) Reuman, D. C.; Anderson, T. L.; Walter, J. A.; Zhao, L.; Sheppard, L. W. wsyn: Wavelet Approaches to Studies of Synchrony in Ecology and Other Fields (R package version 1.0.4), 2021.
(75) *National Atmospheric Deposition Program (NRSP-3). National Trends Network* NADP Program Office, Wisconsin State Laboratory of Hygiene: Madison, WI; 2023.
(76) PRISM Group. *Parameter-elevation Regressions on Independent Slopes Model* Oregon State University: Corvallis, OR; 2023.
(77) Edmund, H.; Bell, K.; Butler, A. prism: Access Data from the Oregon State Prism Climate Project (R package version 0.2.1), 2023.
(78) *POWER Project. Prediction of Worldwide Energy Resources* National Aeronautics and Space Administration (NASA) Langley Research Center (LaRC): Hampton, VA; 2023.
(79) Sparks, A. H.; Chamberlain, S.; Kavili, H.; Boyer, A.; Miguez, F.; Salmon, M.; Alderman, P. D.; Blagotić, A.; Daróczi, G.; Curtin University nasapower: NASA POWER API Client (R package version 4.2.2), 2024.
(80) Sparks, A. H. nasapower: A NASA POWER global meteorology, surface solar energy and climatology data client for R. *J. Open Source Software* **2018**, *3* (30), No. 1035.
(81) Walter, J. A.; Coombs, N. J.; Pace, M. L. Synchronous variation of dissolved organic carbon in Adirondack lakes at multiple timescales. *Limnol. Oceanogr. Lett.* **2023**, *8* (4), 649−656.
(82) Sheppard, L. W.; Bell, J. R.; Harrington, R.; Reuman, D. C. Changes in large-scale climate alter spatial synchrony of aphid pests. *Nat. Clim. Change* **2016**, *6* (6), 610−613.
(83) Walter, J. A.; Fleck, R.; Kastens, J. H.; Pace, M. L.; Wilkinson, G. M. Temporal coherence between lake and landscape primary productivity. *Ecosystems* **2021**, *24* (3), 502−515.
(84) Hirsch, R. M.; Slack, J. R.; Smith, R. A. Techniques of trend analysis for monthly water quality data. *Water Resour. Res.* **1982**, *18* (1), 107−121.
(85) Hussain, M.; Mahmud, I. pyMannKendall: A python package for non parametric Mann Kendall family of trend tests. *J. Open Source Software* **2019**, *4* (39), No. 1556.
(86) Hipel, K. W.; McLeod, A. I. Nonparametric Tests for Trend Detection. In *Time Series Modelling of Water Resources and Environmental Systems*; Hipel, K. W.; McLeod, A. I., Eds.; Elsevier: Amsterdam, Netherlands, 1994; Vol. *45*, Chapter 23, pp 853−938.
(87) Rodríguez-Cardona, B. M.; Wymore, A. S.; Argerich, A.; Barnes, R. T.; Bernal, S.; Brookshire, E. N. J.; Coble, A. A.; Dodds, W. K.; Fazekas, H. M.; Helton, A. M.; Johnes, P. J.; Johnson, S. L.; Jones, J. B.; Kaushal, S. S.; Kortelainen, P.; López-Lloreda, C.; Spencer, R. G. M.; McDowell, W. H. Shifting stoichiometry: Long-term trends in stream-dissolved organic matter reveal altered C:N ratios due to

https://doi.org/10.1021/acs.est.5c04001
Environ. Sci. Technol. XXXX, XXX, XXX−XXX

history of atmospheric acid deposition. *Global Change Biol.* **2022**, *28* (1), 98−114.
(88) R Core Team. *R: A Language and Environment for Statistical Computing*; R Foundation for Statistical Computing: Vienna, Austria, 2024.
(89) Wood, S. N. mgcv: Mixed GAM Computation Vehicle with Automatic Smoothness Estimation (R package version 1.9.1), 2023.
(90) Zhang, J.; Hudson, J.; Neal, R.; Sereda, J.; Clair, T.; Turner, M.; Jeffries, D.; Dillon, P.; Molot, L.; Somers, K.; Hesslein, R. Long-term patterns of dissolved organic carbon in lakes across eastern Canada: Evidence of a pronounced climate effect. *Limnol. Oceanogr.* **2010**, *55* (1), 30−42.
(91) Canham, C. D.; Pace, M. L.; Papaik, M. J.; Primack, A. G. B.; Roy, K. M.; Maranger, R. J.; Curran, R. P.; Spada, D. M. A spatially explicit watershed-scale analysis of dissolved organic carbon in Adirondack lakes. *Ecolo. Appl.* **2004**, *14* (3), 839−854.
(92) Sobek, S.; Tranvik, L. J.; Prairie, Y. T.; Kortelainen, P.; Cole, J. J. Patterns and regulation of dissolved organic carbon: An analysis of 7,500 widely distributed lakes. *Limnol. Oceanogr.* **2007**, *52* (3), 1208−1219.
(93) Zwart, J. A.; Sebestyen, S. D.; Solomon, C. T.; Jones, S. E. The influence of hydrologic residence time on lake carbon cycling dynamics following extreme precipitation events. *Ecosystems* **2017**, *20* (5), 1000−1014.
(94) Bertilsson, S.; Tranvik, L. J. Photochemical transformation of dissolved organic matter in lakes. *Limnol. Oceanogr.* **2000**, *45* (4), 753−762.
(95) Koehler, B.; Broman, E.; Tranvik, L. J. Apparent quantum yield of photochemical dissolved organic carbon mineralization in lakes. *Limnol. Oceanogr.* **2016**, *61* (6), 2207−2221.
(96) Kalbitz, K.; Solinger, S.; Park, J. H.; Michalzik, B.; Matzner, E. Controls on the dynamics of dissolved organic matter in soils: A review. *Soil Sci.* **2000**, *165* (4), 277−304.
(97) Evans, C. D.; Jones, T. G.; Burden, A.; Ostle, N.; Zieliński, P.; Cooper, M. D. A.; Peacock, M.; Clark, J. M.; Oulehle, F.; Cooper, D.; Freeman, C. Acidity controls on dissolved organic carbon mobility in organic soils. *Global Change Biol.* **2012**, *18* (11), 3317−3331.
(98) Lawrence, G. B.; Roy, K. M. Ongoing increases in dissolved organic carbon are sustained by decreases in ionic strength rather than decreased acidity in waters recovering from acidic deposition. *Sci. Total Environ.* **2021**, *766*, No. 142529.
(99) Cronan, C. S.; Aiken, G. R. Chemistry and transport of soluble humic substances in forested watersheds of the Adirondack Park, New York. *Geochim. Cosmochim. Acta* **1985**, *49* (8), 1697−1705.
(100) Piatek, K. B.; Christopher, S. F.; Mitchell, M. J. Spatial and temporal dynamics of stream chemistry in a forested watershed. *Hydrol. Earth Syst. Sci.* **2009**, *13* (3), 423−439.
(101) Zarnetske, J. P.; Bouda, M.; Abbott, B. W.; Saiers, J.; Raymond, P. A. Generality of hydrologic transport limitation of watershed organic carbon flux across ecoregions of the United States. *Geophys. Res. Lett.* **2018**, *45* (21), 11702−11711.
(102) Hall, L. J.; Emilson, E. J. S.; Edwards, B.; Watmough, S. A. Patterns and trends in lake concentrations of dissolved organic carbon in a landscape recovering from environmental degradation and widespread acidification. *Sci. Total Environ.* **2021**, *765*, No. 142679.
(103) Dawson, J. J. C.; Malcolm, I. A.; Middlemas, S. J.; Tetzlaff, D.; Soulsby, C. Is the composition of dissolved organic carbon changing in upland acidic streams? *Environ. Sci. Technol.* **2009**, *43* (20), 7748−7753.
(104) Jane, S. F.; Winslow, L. A.; Remucal, C. K.; Rose, K. C. Long-term trends and synchrony in dissolved organic matter characteristics in Wisconsin, USA, lakes: Quality, not quantity, is highly sensitive to climate. *J. Geophys. Res.: Biogeosci.* **2017**, *122* (3), 546−561.
(105) Pugh, E. A.; Olefeldt, D.; Leader, S. N.; Hokanson, K. J.; Devito, K. J. Characteristics of dissolved organic carbon in boreal lakes: High spatial and inter-annual variability controlled by landscape attributes and wet-dry periods. *Water Resour. Res.* **2021**, *57* (11), No. e2021WR030021.
(106) Hood, E.; Gooseff, M. N.; Johnson, S. L. Changes in the character of stream water dissolved organic carbon during flushing in three small watersheds, Oregon. *J. Geophys. Res.: Biogeosci.* **2006**, *111* (G1), No. G01007.
(107) Vidon, P.; Wagner, L. E.; Soyeux, E. Changes in the character of DOC in streams during storms in two Midwestern watersheds with contrasting land uses. *Biogeochemistry* **2008**, *88* (3), 257−270.
(108) Berggren, M.; Guillemette, F.; Bieroza, M.; Buffam, I.; Deininger, A.; Hawkes, J. A.; Kothawala, D. N.; LaBrie, R.; Lapierre, J.-F.; Murphy, K. R.; Al-Kharusi, E. S.; Rulli, M. P. D.; Hensgens, G.; Younes, H.; Wünsch, U. J. Unified understanding of intrinsic and extrinsic controls of dissolved organic carbon reactivity in aquatic ecosystems. *Ecology* **2022**, *103* (9), No. e3763.
(109) McCabe, A. J.; Arnold, W. A. Seasonal and spatial variabilities in the water chemistry of prairie pothole wetlands influence the photoproduction of reactive intermediates. *Chemosphere* **2016**, *155*, 640−647.
(110) Maizel, A. C.; Li, J.; Remucal, C. K. Relationships between dissolved organic matter composition and photochemistry in lakes of diverse trophic status. *Environ. Sci. Technol.* **2017**, *51* (17), 9624−9632.
(111) Chen, Y.; Hozalski, R. M.; Olmanson, L. G.; Page, B. P.; Finlay, J. C.; Brezonik, P. L.; Arnold, W. A. Prediction of photochemically produced reactive intermediates in surface waters via satellite remote sensing. *Environ. Sci. Technol.* **2020**, *54* (11), 6671−6681.
(112) Berg, S. M.; Wammer, K. H.; Remucal, C. K. Dissolved organic matter photoreactivity is determined by its optical properties, redox activity, and molecular composition. *Environ. Sci. Technol.* **2023**, *57* (16), 6703−6711.
(113) Guo, Z.; Wang, T.; Chen, G.; Wang, J.; Fujii, M.; Yoshimura, C. Apparent quantum yield for photo-production of singlet oxygen in reservoirs and its relation to the water matrix. *Water Res.* **2023**, *244*, No. 120456.
(114) Dalrymple, R. M.; Carfagno, A. K.; Sharpless, C. M. Correlations between dissolved organic matter optical properties and quantum yields of singlet oxygen and hydrogen peroxide. *Environ. Sci. Technol.* **2010**, *44* (15), 5824−5829.
(115) Partanen, S. B.; Erickson, P. R.; Latch, D. E.; Moor, K. J.; McNeill, K. Dissolved organic matter singlet oxygen quantum yields: Evaluation using time-resolved singlet oxygen phosphorescence. *Environ. Sci. Technol.* **2020**, *54* (6), 3316−3324.
(116) Paul, A.; Hackbarth, S.; Vogt, R. D.; Roder, B.; Burnison, B. K.; Steinberg, C. E. W. Photogeneration of singlet oxygen by humic substances: Comparison of humic substances of aquatic and terrestrial origin. *Photochem. Photobiol. Sci.* **2004**, *3* (3), 273−280.
(117) McKay, G.; Huang, W.; Romera-Castillo, C.; Crouch, J. E.; Rosario-Ortiz, F. L.; Jaffé, R. Predicting reactive intermediate quantum yields from dissolved organic matter photolysis using optical properties and antioxidant capacity. *Environ. Sci. Technol.* **2017**, *51* (10), 5404−5413.
(118) Li, Y.; Zhang, K.; Apell, J.; Ruan, Y.; Huang, X.; Nah, T. Photoproduction of reactive intermediates from dissolved organic matter in coastal seawater around an urban metropolis in South China: Characterization and predictive modeling. *Sci. Total Environ.* **2024**, *921*, No. 170998.
(119) Glover, C. M.; Rosario-Ortiz, F. L. Impact of halides on the photoproduction of reactive intermediates from organic matter. *Environ. Sci. Technol.* **2013**, *47* (24), 13949−13956.
(120) Zhou, H.; Yan, S.; Lian, L.; Song, W. Triplet-state photochemistry of dissolved organic matter: Triplet-state energy distribution and surface electric charge conditions. *Environ. Sci. Technol.* **2019**, *53* (5), 2482−2490.
(121) Grandbois, M.; Latch, D. E.; McNeill, K. Microheterogeneous concentrations of singlet oxygen in natural organic matter isolate solutions. *Environ. Sci. Technol.* **2008**, *42* (24), 9184−9190.
(122) Cheng, K.; Zhang, L.; McKay, G. Evaluating the micro-heterogeneous distribution of photochemically generated singlet

https://doi.org/10.1021/acs.est.5c04001
Environ. Sci. Technol. XXXX, XXX, XXX−XXX

oxygen using furfuryl amine. *Environ. Sci. Technol.* **2023**, *57* (19), 7568−7577.
(123) Frimmel, F. H.; Bauer, H.; Putzien, J.; Murasecco, P.; Braun, A. M. Laser flash photolysis of dissolved aquatic humic material and the sensitized production of singlet oxygen. *Environ. Sci. Technol.* **1987**, *21* (6), 541−545.
(124) Wan, D.; Sharma, V. K.; Liu, L.; Zuo, Y.; Chen, Y. Mechanistic insight into the effect of metal ions on photogeneration of reactive species from dissolved organic matter. *Environ. Sci. Technol.* **2019**, *53* (10), 5778−5786.
(125) Cory, R. M.; Kling, G. W. Interactions between sunlight and microorganisms influence dissolved organic matter degradation along the aquatic continuum. *Limnol. Oceanogr. Lett.* **2018**, *3* (3), 102−116.
(126) Wasswa, J.; Driscoll, C. T.; Zeng, T. Contrasting impacts of photochemical and microbial processing on the photoreactivity of dissolved organic matter in an Adirondack Lake watershed. *Environ. Sci. Technol.* **2022**, *56* (3), 1688−1701.
(127) McDonough, L. K.; Andersen, M. S.; Behnke, M. I.; Rutlidge, H.; Oudone, P.; Meredith, K.; O'Carroll, D. M.; Santos, I. R.; Marjo, C. E.; Spencer, R. G. M.; McKenna, A. M.; Baker, A. A new conceptual framework for the transformation of groundwater dissolved organic matter. *Nat. Commun.* **2022**, *13* (1), No. 2153.
(128) Gerson, J. R.; Driscoll, C. T.; Roy, K. M. Patterns of nutrient dynamics in Adirondack lakes recovering from acid deposition. *Ecol. Appl.* **2016**, *26* (6), 1758−1770.
(129) Du, Z.; He, Y.; Fan, J.; Fu, H.; Zheng, S.; Xu, Z.; Qu, X.; Kong, A.; Zhu, D. Predicting apparent singlet oxygen quantum yields of dissolved black carbon and humic substances using spectroscopic indices. *Chemosphere* **2018**, *194*, 405−413.
(130) Wood, S. N. *Generalized Additive Models: An Introduction with R*, 2nd ed.; Chapman and Hall/CRC: New York, 2017.
(131) Wasswa, J.; Driscoll, C. T.; Zeng, T. Photochemical characterization of surface waters from lakes in the Adirondack Region of New York. *Environ. Sci. Technol.* **2020**, *54* (17), 10654−10667.
(132) Wasswa, J.; Perkins, M.; Matthews, D. A.; Zeng, T. Characterizing the impact of cyanobacterial blooms on the photoreactivity of surface waters from New York lakes: A combined statewide survey and laboratory investigation. *Environ. Sci. Technol.* **2024**, *58* (18), 8020−8031.
(133) Sharpless, C. M.; Blough, N. V. The importance of charge-transfer interactions in determining chromophoric dissolved organic matter (CDOM) optical and photochemical properties. *Environ. Sci.: Processes Impacts* **2014**, *16* (4), 654−671.
(134) Wang, S.; Matt, M.; Murphy, B. L.; Perkins, M.; Matthews, D. A.; Moran, S. D.; Zeng, T. Organic micropollutants in New York lakes: A statewide citizen science occurrence study. *Environ. Sci. Technol.* **2020**, *54* (21), 13759−13770.
(135) Dittman, J. A.; Driscoll, C. T. Factors influencing changes in mercury concentrations in lake water and yellow perch (Perca flavescens) in Adirondack lakes. *Biogeochemistry* **2009**, *93* (3), 179−196.
(136) Gorney, R. M.; June, S. G.; Stainbrook, K. M.; Smith, A. J. Detections of cyanobacteria harmful algal blooms (cyanoHABs) in New York State, United States (2012−2020). *Lake Reserv. Manage.* **2023**, *39* (1), 21−36.
(137) Hanna, M. Evaluation of models predicting mixing depth. *Can. J. Fish. Aquat. Sci.* **1990**, *47* (5), 940−947.
(138) Pickett, S. T. A. Space-for-Time Substitution as an Alternative to Long-Term Studies. In *Long-Term Studies in Ecology: Approaches and Alternatives*; Likens, G. E., Ed.; Springer: New York, NY, 1989; pp 110−135.
(139) Stetler, J. T.; Knoll, L. B.; Driscoll, C. T.; Rose, K. C. Lake browning generates a spatiotemporal mismatch between dissolved organic carbon and limiting nutrients. *Limnol. Oceanogr. Lett.* **2021**, *6* (4), 182−191.
(140) Eklöf, K.; von Brömssen, C.; Amvrosiadi, N.; Fölster, J.; Wallin, M. B.; Bishop, K. Brownification on hold: What traditional analyses miss in extended surface water records. *Water Res.* **2021**, *203*, No. 117544.
(141) McNeill, K.; Canonica, S. Triplet state dissolved organic matter in aquatic photochemistry: Reaction mechanisms, substrate scope, and photophysical properties. *Environ. Sci.: Processes Impacts* **2016**, *18* (11), 1381−1399.
(142) Page, S. E.; Arnold, W. A.; McNeill, K. Assessing the contribution of free hydroxyl radical in organic matter-sensitized photohydroxylation reactions. *Environ. Sci. Technol.* **2011**, *45* (7), 2818−2825.

https://doi.org/10.1021/acs.est.5c04001
Environ. Sci. Technol. XXXX, XXX, XXX−XXX